DISLOCATIONS IN GALLIUM ARSENIDE DEFORMED AT HIGH TEMPERATURES

By

PATRICK JOHN GALLAGHER

B.A.Sc. The University of British Columbia, 1983

A THESIS SUBMITTED IN PARTIAL FULFILLMENT OF

THE REQUIREMENTS FOR THE DEGREE OF

MASTER OF APPLIED SCIENCE

in

THE FACULTY OF GRADUATE STUDIES

(Metals and Materials Engineering)

We accept this thesis as conforming

to the required standard

THE UNIVERSITY OF BRITISH COLUMBIA

April 1987

In presenting this thesis in partial fulfilment of the requirements for an advanced degree at the University of British Columbia, I agree that the Library shall make it freely available for reference and study. I further agree that permission for extensive copying of this thesis for scholarly purposes may be granted by the head of my department or by his or her representatives. It is understood that copying or publication of this thesis for financial gain shall not be allowed without my written permission.

Department of METALS AND MATERIALS ENGINEERING

The University of British Columbia
1956 Main Mall
Vancouver, Canada
V6T 1Y3

Date 29 APRIL 1987

Abstract

Test pieces of GaAs were cut from Czochralski grown <100> wafers. Prior to deformation the dislocation configuration was established by cathodoluminescence (CL). Etch pits produced by molten KOH on examined crystal surfaces coincided with the CL images. The test pieces were capped with Si_3N_4, heated to between 950 and 1050°C, and plastically deformed by bending. The dislocation configuration after bending was then compared to that of the undeformed crystal.

It was observed that heating to 1050°C did not significantly change the as grown cellular dislocation arrays in the crystal. With strain the dislocation configuration changed appreciably. New bands of dislocations were formed, parallel to the bend axis with dislocation free regions between them. Increasing the strain increased the number of bands. Observations were made on undoped crystals with high and low dislocation densities, and Si doped crystals.

The luminescent properties of the dislocations were observed to change with heating and strain. As grown, a dislocation imaged as a dark spot surrounded by a bright halo, giving bright dislocation networks. After heating to 950°C samples showed only the dark spots without halos. After deformation, all the new dislocations appeared as dark spots or lines without halos. At

very low strains, the original dislocations were still evident but were distinct from the new arrays.

In an attempt to correlate the dislocation images with impurity segregation some observations of the samples were made using secondary ion mass spectroscopy (SIMS). The results suggest the possibility of the dark areas in the CL images being associated with the presence of carbon.

Table of Contents

List of Tables

List of Figures

Acknowledgement

The work described in this thesis and the manuscript were prepared under the auspices of Dr. F. Weinberg. Financial support was provided, in part, by a fellowship from Alcan. Thanks are also extended to the faculty and staff at U.B.C. metallurgy for their assistance.

Special thanks are extended to faculty and staff at B.C.I.T. Physics for their support and access to equipment for preparing this manuscript.

Finally, to my wife Diana, without whose support this work would not have been completed, a very special thanks.

1 Introduction

Commercially produced gallium arsenide (GaAs) is finding application in integrated opto-electronic systems due to its semiconducting and optical properties. The crystals, as grown by the liquid encapsulated Czochraloski (LEC) process, contain a high concentration of dislocations relative to silicon, usually formed into cellular arrays. These dislocations are suspect in the low yield of integrated circuits from GaAs wafers. In particular, the dislocations are known to be the cause of failure of optical devices (lasers) built onto the wafer. Attempts to reduce the number of dislocations in the as-grown crystals are ongoing. Attempts at removing or reorganizing the dislocation networks by annealing the wafers (or boules) have been unsuccessful.

The purpose of this work was to determine whether the arrays of grown-in dislocations in GaAs could be moved with application of temperature and strain. Further, if they could be moved, then determine if they could be moved into regular arrays, and the critical parameters to accomplish this. To make these observations required a technique for delineating the dislocations in GaAs. This could be attempted using several techniques.

1.1 Literature Review

Previous deformation studies on GaAs have involved the determination of macroscopic properties such as yield strength as a function of temperature[1,2]. In reference (1) specimens of GaAs were deformed by bending up to 700°C in air and in tension from 700 to 1000°C in an arsenic (As) atmosphere. After deformation the sample surface was etched in molten potassium hydroxide (KOH) to reveal the dislocation arrangement. Some samples were also prepared for examination in a transmission electron microscope (TEM). In a typical test, deformation reached 10 to 20 per cent, and the resulting dislocation densities were on the order of $10^8/cm^2$. The dislocations were found to be aligned on the intersection of {111} planes with the surface. The slip system was determined as {111}<110> and the majority of dislocations had Burgers vectors of $\frac{a}{2}$<110>.

In reference (2) the mechanical properties of GaAs were investigated with respect to the use of GaAs as an infra red (ir) window. The study considered yield strength and fracture behaviour in compressively loaded specimens oriented with either <111> or <100> along the compressed axis over the temperature range of 250 to 550°C. Samples of undoped and Si, Cr, or Zn doped GaAs were tested. The samples were loaded at constant loading rates of 13.7, 34.3, and 68.7 MPa/s. Specimens were placed between Al_2O_3 buttons inside a three zone furnace.

A thermocouple was placed against the specimen to record temperature. Load and crosshead displacement were recorded and the resulting stress-strain curves are shown in Figure 1 for the <100> and Figure 2 for the <111> oriented Si doped specimens.

The results confirmed a slip system of {111}<110> since the ratio of yield strengths of <111> and <100> oriented samples, over the temperature range, was constant. Multiplying each set of data by their appropriate Schmid factors collapsed the data onto one curve of critical resolved shear stress (CRSS) versus temperature for the Si doped samples.

The study also showed a monotonic decrease in yield strength with temperature for all doping species and undoped GaAs as shown in Figure 3 of yield stress versus temperature for <100> oriented specimens. It was found that Si doping increased the yield strength, Zn doping lead to a drop in yield strength, and Cr doping did not seem to affect the yield strength.

All tests were conducted in air. Samples were strained to levels of 10 to 20 per cent. The maximum test temperature was limited to 550°C to avoid problems associated with As loss from the surface of the GaAs specimens.

Microscopic studies of dislocation movement associated with small stresses have also been undertaken[3,4]. In these works the

effects on dislocation velocity, of stress, temperature, and irradiation (electron beam) level were studied. In reference (3) a series of heating and stressing experiments were carried out inside a scanning electron microscope (SEM) that had been equipped with cathodoluminescence (CL) detection apparatus. A damaged area was introduced into the GaAs surface by a diamond scribe. This generated the dislocations which were subsequently studied. By careful manipulation of the GaAs specimen and the electron beam scan area, a condition of stress and localized irradiation (electron beam) was used to pull a single dislocation out from the damaged region. Once this had been accomplished, states of uniform heating, irradiation, and stress were applied and the dislocation was tracked in the CL image.

The bending apparatus was a four point system (generates constant bending moment in the centre span, ie. constant surface stress) driven by a solenoid. The load was controlled by the amount of current passing through the solenoid windings and had the facility to be either held at a constant load or cycled at various frequencies. The solenoid and magnetic core were enclosed in an aluminum case to shield the SEM from the magnetic field generated. The bending jig itself was surrounded by shielded heating coils which were used to control the temperature of the specimen. Temperatures were recorded from thermocouples placed in contact with the GaAs specimen.

The positions of the dislocations were recorded from the CL image as a function of time at temperature, irradiation, and stress level. A typical set of data taken at 195°C and a stress level of 47MPa is shown in Figure 4. The dislocation velocity is the slope of this plot and this was the parameter measured against temperature, irradiation, and stress. Two of these were held constant while the third was varied.

Accumulated results showed a range of dislocation velocities from 10^{-9} to 10^{-6}m/s, between 27 and 427°C, with stress levels from 10 to 50MPa and irradiation from 30keV electrons at current densities from 4×10^{-3} to 5×10^{-1}A/m^2.

At temperatures above 227°C the background radiation was sufficient to flood the CL detector, so continuous imaging was not possible. Instead images were taken before and after specific times at stress and temperature. The highest temperature that could be studied was restricted to that below which degradation of the GaAs surface, due to loss of As, was a problem. Therefore the highest temperature studied was limited to 427°C. This study was not directly concerned with the grown-in arrays of dislocations.

1.2 Gallium Arsenide

In its crystalline form GaAs has a cubic zinc blende structure with a lattice constant (a) of 5.65Å. The lattice can be interpreted as two inter-penetrating face-centred-cubic (FCC) lattices, one of Ga, the other of As, offset from each other by a quarter of a lattice spacing ($\frac{a}{4}$<111>). Figure 5 shows the unit cube of the crystal. The larger circles (As) are shown on the FCC sites of the unit cube. The smaller filled circles (Ga) are those atoms inside the unit cube while the smaller open circles (Ga) show the remainder of the second FCC lattice outside the unit cube.

The crystal is a semiconductor and in the undoped state it is semi-insulating. It is a direct band gap semiconductor with a room temperature (300K) band gap of 1.423eV. Figure 6 compares the direct gap (conduction band minimum directly above the valance band maximum in k space) band structure of GaAs with the indirect gap structure of Si or Ge. A photon emitted from GaAs due to a simple electron-hole recombination has a wavelength of 871nm. Recombination can take place anywhere across the gap however, with the proper phonons available, and so a more typical wavelength of 838nm is observed for GaAs[5].

Mechanically the crystal is quite brittle at room temperature but will deform by slip on {111}<110> at elevated

temperatures. Its density is $5.317\times10^{3}kg/m^{3}$. The melting point is 1238°C and the specific heat at 300K is 327J/kg·K. The linear coefficient of thermal expansion is 5.73×10^{-6} at 300K. GaAs dissociates at temperatures over 450°C due to the rise of the partial pressure of the As. This complicates both the growth of the crystals and also high temperature experiments on GaAs.

1.3 Cathodoluminescence

One of the signals that is generated from the GaAs specimen as a result of bombardment by the electron beam of the SEM is cathodoluminescence (CL). The CL signal results from the recombination of the excess hole-electron pairs generated by the impinging electron beam. As each pair recombines they lose their energy of formation, equal to the difference in the excited band energies and the rest energy. This difference is usually equal to the band gap. Figure 7 shows a schematic of the energy band structure of GaAs and the simplest recombination scenario. The lost energy can be released as a photon, and this has a high probability for a direct band gap crystal such as GaAs.

In regions of the crystal where there are inter band energy levels (traps) available due to the presence of foreign atoms or dislocations, the recombination can still take place but with a different wavelength photon or without any photon being released. A schematic of the process in which an electron drops from the

conduction band to an inter band level is shown in Figure 8. The photon released is lower in energy (has a longer wavelength) than the one released when an electron falls across the whole gap. This effect produces the contrast in the CL images. The CL detector can be chosen to be most sensitive to the wavelength emitted by the crystal as a whole (ie. $E_{ph} = E_{gap}$). Areas that emit photons of other wavelengths or emit no photons will therefore appear darker with this detector. As a result, regions of the crystal that do not contain foreign atoms (dopants or contaminants) or dislocations will have a brighter local CL image, and regions that do contain impurities and/or dislocations will have a darker local CL image.

Dislocations, which interfere with the normal luminescence of the crystal, appear as dark spots or lines in CL images. These spots (lines) are called "dark spot(line) defects" (DS(L)Ds) and have been observed in degraded opto-electronic devices[3]. Further observations showed these DSDs coincided with the etch pit configuration on an etched GaAs crystal and therefore the dislocation distribution. Correlations between CL images and dislocation revealing etch pits have previously been shown[6] and are demonstrated in this work.

Evidence that some of the contrast in CL images that depicts the dislocation sites is related to the level of trace impurities that have accumulated around the grown-in dislocations has been

demonstrated[7]. This was accomplished by assessing the local impurity level using secondary ion mass spectrometry (SIMS) and comparing the distribution of contaminants with the CL images of the dislocation networks. Residuals of Si, O, Cr, and C were all found to be concentrated at the dislocation cell walls in undoped, semi-insulating GaAs. The resolution available could not register the concentration difference between the dislocation cores and the region immediately surrounding.

1.4 Observing Dislocation Arrangements

To examine the dislocation configuration before and after heating and deformation requires two sets of observations of the same area. One way of doing this is to etch the crystal in an etchant which reveals the dislocations at the surface as pits. The specimen is then polished to remove the pits, heated, deformed, and then re-etched to delineate the new dislocation arrangement. The process of etching and re-etching is time consuming and is destructive to the crystal. In the case of GaAs, and other direct band gap semiconductors, an alternatative procedure is possible. Dislocations at or near the surface can be observed by imaging the CL signal emitted from the crystal.

2 Procedures

Test plates of GaAs were deformed at high temperatures. Two jigs were designed and fabricated in order to deform the GaAs specimens at the high temperatures inside a crystal grower. The GaAs specimens required preparation involving cleaning, polishing, and capping to protect their surfaces during heating. The specimens were characterized before heating and deformation tests, and re-examined afterwards. An Etec SEM was modified to be used as a CL imaging device in order to characterize GaAs specimens with respect to dislocation arrangement and density.

2.1 Deformation of GaAs Plates

Samples of GaAs were prepared and loaded into specially designed three point bending jigs. The jig and specimen were then placed inside a GaAs crystal grower. The grower chamber was then sealed and flushed with argon. After two evacuations and back fills with argon the chamber was pressurized to approximately 2kPa. Concurrently with this the cooling water was turned on and allowed to circulate. After the flow had stabilized the cooling lines were bled to release any trapped air. The set point of the growers heater controller was set to approximately 220C° below the desired test temperature (900°C to 1050°C) and power was applied to the heaters using the automatic control mode. When the thermocouple indicated the maximum

overshoot (approximately 200C°) the set point was reset to the overshoot temperature and the grower was left to stabilize for 300 seconds. The set point was then increased in steps to the desired test temperature using a rate of 0.033°C/s. At the desired temperature the grower was left to stabilize for 600 seconds. At this point the deformation was carried out which involved centre deflections of between 0.25mm and 1.0mm. The samples were loaded in either a static manner, which left them in the bent state, or in a cyclic manner through 1 to 5 cycles. At the conclusion of the deformation treatment the samples were allowed to anneal for 90 to 600 seconds at the test temperature. The cooling sequence was accomplished by reducing the controller set point by 200C° at a time and allowing the temperature offset to go to zero before the next reduction. The temperature controller maintained about a 10 per cent of maximum input power during this phase of cooling. After cooling to a temperature of 300°C the power to the heaters was turned off and the grower was allowed to cool to room temperature with the cooling water. Throughout the heating, bending, and cooling the pressure in the chamber was maintained at the 2kPa by controlling both the argon inlet flow rate and the chamber outlet flow rate. The specimen and jig were observed through the viewing port of the grower chamber.

After the chamber had cooled completely, the cooling water was turned off, residual pressure in the chamber was bled off,

and the chamber was opened. The jig was removed from the grower and the GaAs specimen was recovered from the jig. All parts were handled with gloved hands due to the presence of As dust and masks were worn during recovery (and loading) for the same reason. The specimens were handled by the edges with tweezers and place in covered petri dishes containing ethyl alcohol.

The test pieces of GaAs were then prepared for CL examination. This was accomplished by a series of polishes and rinses, to be described later, and finally mounting on the specimen holder for the examination. The mounted samples were placed in an Etec SEM that had been modified to image CL signals. The dislocation arrangement in the sample was imaged by CL and these image were compared with the CL images taken from the same areas on the specimen before the heating and deformation.

Table I shows a compilation of all the specimens tested and the test conditions.

sample #	from wafer #	capping Si_3N_4 (Å)	Tmax (°C)	deflection (mm)	cycles (#,rate)	anneal (s)
T1	44	750	955	0.2	static	120
T2	44	750	955	1.0	static	120
T3	44	750	955	0.5	static	60
T4	44	750	955	0	static	600
T5	44	750	955	0.4	static	600
Si1	273#45	750	955	0.25	static	60
L1	293#9	750	955	0.25	static	60
S1	1214S61	800	1000	0.5	5,high	30
S2	1214S61	800	1050	0.5	4,high	120
S3	1214S61	800	1000	0.25	1,low	90
S4	1214S61	800	1000	0.25	3,low	120

deflection rates : high = 0.21mm/s low = 0.014mm/s
thicknesses : Com. J#44 = 0.40mm Com. EG#1214S61 = 0.49mm
HP 273#45 = 0.48mm HP293#9 = 0.434mm

TABLE I. GaAs specimens and test conditions.

2.2 Bending Jigs

Two jigs for bending the GaAs were designed and employed. The first was a static bending jig used in early experiments to find the range of temperatures where GaAs deformed plastically. The second, dynamic jig deformed the GaAs in cyclic bending under controlled strain.

In order to minimize the effect of the thermal gradient across the chamber the apparatus was made sufficiently small to occupy only the centre region of the crucible. The use of small bending jigs also minimized the cost of both jig materials and GaAs specimens, that is, more could be made from the same quantity of stock.

2.21 Static Bending Jig

The static bending jig is shown schematically in Figure 9a. It consists of a large support block "A" of boron nitride (BN) with a recess cut for one end of the 25mm long specimens "B" and provision for the stainless steel (type 316) mass and strain control block "C". A half round of BN "D" was cut to the same height as the recess in the support block and provided the central bearing load for the specimen. A small cylinder of BN "E" contained a slot for the cantilever end of the GaAs specimen and provided the load on the end of the specimen. The load block "E" was kept in alignment by a vertical stainless steel guide rod "F". The guide rod runs in the stainless steel guides "G" attached to "C" preventing the specimen from twisting. It also serves as an indicator of specimen deflection, since bending of the specimen inclines the rod, causing the top of the rod to move horizontally, magnifying the sample deflection by the bar length. The load applied to the specimen could be increased readily by adding washers onto block "E", held in place by the vertical rod. The guides themselves are attached to "C" by a locking screw and can be extended or retracted to give various amounts of strain to the specimens.

Three bending systems were built into the jig (shown in Figure 9b) which then allowed three samples to be tested simultaneously under the same thermal and environmental conditions. In a given test, variables between specimens considered were specimen material, applied load, and maximum strain.

2.22 Dynamic Bending Jig

The dynamic bending jig was designed for cyclic strain testing and is shown in section in Figure 10. The jig has a three point bending system with devices for strain limitation The jig consists of a main body "A" that holds two lower support pins "B" and a movable top piece "C" that contains the central loading pin "D", the return block "E" and the strain control "F" and "G". A mass ring "I", made of stainless steel, provides the downward load during a return cycle.

The jig was designed to bend the specimen a controlled amount on loading and then to pull the specimen back to its initial position without an excess of compressive loading. This can be done once, or several times, in a given test at various temperatures, strain(loading) rates and maximum strain values. For this jig loading was carried out through "G" by an external source, the seed lift mechanism.

2.23 Materials Selection

Materials for the bending apparatus were selected based on a number of factors. (1) The device had to perform mechanically at high temperature, without seizing or galling. (2) A low coefficient of thermal expansion was required so that cold set clearances and limits would not vary over the temperature range of interest. (3) The device had to be unaffected by GaAs or As at high temperatures. (4) There could be no reaction between the material and GaAs at high temperatures. The material chosen was HP grade boron nitride (BN).

Pyrolitic BN is the material employed as the crucible for containing the molten GaAs during growth of crystals in commercial growing operations. The compound, BN, is therefore, suitably inert to and from GaAs. BN is a non-seizing material when used against itself, and remains self lubricating to over 1600°C. It retains its mechanical strength to over 2700°C, and is easily machinable to a 4-5 micron finish, but is brittle. HP grade BN has a specified coefficient of thermal expansion of 0.0×10^{-6} from 75°C to over 1000°C. BN is susceptible to damage by absorption of moisture which results in a drop in strength. HP grade BN has a small amount of Ca added to it to minimize the effects of moisture.

2.24 Strain Calibration of Dynamic Jig

The maximum strain imposed on the specimen is limited by the strain limiting block "F". When this block reaches the top face of the lower assembly block "A" there is no further downward movement of the loading pin. To set the maximum strain, a shim of thickness equal to the desired maximum strain is placed between the limiter block "F" and the top face of the lower assembly "A". With a specimen in place the strain adjustment screw can be adjusted so that the centre pin just contacts the specimen surface at the end of the downward travel. For a bend test the shim is removed and the additional downward travel now available is the shim thickness. In actual practice the condition of the centre pin "just contacting" the specimen is difficult to assess. There is a further complication in that some measure of downward load must be applied during the strain limit adjustment to take up the necessary clearances and tolerances that allow the jig to move. This needed downward load would be hazardous to the GaAs specimens which are very brittle at room temperature; a small deflection applied during the adjustment would break the GaAs specimen.

In order to circumvent these difficulties a long, flexible pseudo specimen was substituted for the GaAs specimen during the strain limit adjustment. This pseudo specimen was chosen long enough so that roughly half its length extended outside the jig.

The long extension provided a mechanical amplification of the centre displacement which was needed to determine zero centre deflection. That is, the extended tip is displaced proportionately to the centre deflection but at a higher rate. The condition of "just contacting" the specimen is now translated into a zero deflection at the end of the extended portion of the pseudo specimen.

A 50mm long, 0.5mm diameter graphite rod was chosen as the pseudo specimen. After adjustment, the locking nut was tightened onto the adjusting screw. A confirmation that the desired centre deflection would actually be realized is accomplished by removing the shim and applying the deflection to the graphite rod. The slope of the extended portion of the rod can then be used to calculate the actual centre deflection. This was in agreement with the shim thickness. The actual strain seen by the GaAs specimen was different than that for the graphite rod by an amount equal to the difference in the thickness of the two, this was taken into account when selecting the shim.

2.3 Environmental Conditions

At higher temperatures the vapour pressure of As in the GaAs is increased sufficiently to cause dissociation of the GaAs. This leads to the release of free As into the high temperature environment. Thus, containment of As was a prime concern.

Heating of specimens, even in an inert atmosphere, leads to loss of As from the surface, and a subsequent excess of elemental Ga left behind on the GaAs. Ga is liquid above 32°C. The process leads to the formation of thermal pits into the surface of the GaAs specimen. A major drawback of a small specimen is its relatively large ratio of surface area to volume leading to aggravated deterioration of the specimen by loss of surface As. Protecting the specimen surface from this type of damage was also a major concern.

Therefore, the whole of the experiment had to be carried out in a sealed environment with a mechanical feed-through, a viewing system and capacity to heat the test assembly to better than 1000°C. Based on these requirements, the GaAs crystal grower was chosen as the containment vessel. The grower is suitably designed to deal with the As released from the GaAs as this is a much more severe problem when melting a charge of several kilograms of GaAs as opposed to the small specimens used for deformation experiments. Also, the grower is designed to run at moderate pressures over atmospheric and this serves to reduce the rate of As loss from the surface of the heated GaAs specimen.

The heaters were left in place to provide the high temperatures required. The seed lift mechanism was used to

provide the necessary mechanical feed-through, and the viewing window allowed observation of the experiment.

2.4 Temperature Calibration

In order to carry out high temperature deformation tests on GaAs specimens it was necessary to measure the temperature of the sample during the test. It is difficult to introduce thermocouples into the high pressure growth chamber and position them close to the test sample. As an alternative, the control thermocouple of the crystal grower was calibrated and used to determine the sample temperature thermocouple. The large thermal mass of the system and the necessary stability and repeatability of the control thermocouple made this procedure reasonable.

The thermocouple was calibrated by melting samples of known melting temperatures at the position in the chamber where the deformation tests were to be carried out. Three elements were used as calibrating materials: germanium, silver, and gold. The calibration was run in a quartz crucible at a fixed crucible height of 14cm against the reference bar, using the 15cm heater. Calibrations were conducted at approximately 2kPa, under the same conditions the heating and deformation experiments were carried out.

Three quartz ampules were made from 10mm (OD) tube stock. They were made approximately 5cm long, sealed at one end and necked down to 3mm (ID) in the middle. A small amount of calibrating material was placed in the top half of each ampule. The ampules were flushed with argon then their tops were sealed. The ampules were then placed upright in a cylindrical graphite holder which was then placed in the bottom of the grower crucible. The graphite holder supported the ampules, set them at the correct height above the bottom of the crucible, positioned each ampule the same distance from the centre of the chamber, thus giving the ability to rotate the crucible to bring each ampule into best viewing position, and provided a thermal mass to minimize small temperature transients. After the grower was sealed and pressurized the temperature was slowly raised (0.033°C/s for Ge, Ag and 0.0083°C/s for Au) through the melting points of the three standards. Melting was observed, through the grower chamber window, when the material flowed from the top section of the ampules to the bottom. The melt temperatures could then be related to the output of the control thermocouple (output equals the set point when the offset is zero). This gives a calibration curve of control thermocouple related to the temperature at the centre of the grower chamber. Melting temperatures were believed to be within 1.5°C for all three materials used. The plot of temperature versus controller thermocouple, shown in Figure 11, has excellent linearity

(R^2 = 0.9994) with predictor errors of less than 2°C on all points.

A similar temperature calibration was carried out for the 20cm heater with crucible height of 14cm. The calibration curve obtained is shown in Figure 12. All of the heating and deformation tests were carried out between 900 and 1050°C, this is inside the range of calibration given in Figures 11 and 12. The temperature of the GaAs during a heating and deformation test is believed to be correct to within 10°C of the stated values.

2.5 Specimen Preparation and Handling

Initial tests were carried out on sections cut from low grade wafers of GaAs. These wafers were received in an as cut condition and required a chemical polish in a 15 per cent solution of bromine in methanol for 300 seconds.

2.51 Arsenic Containment

Samples which were to be heated had to be protected from loss of surface arsenic which results in thermal pitting and surface degradation. Initial attempts were made to prevent arsenic loss by heating the specimens under a layer of boron oxide (B_2O_3). This is the material used as the liquid encapsulant during the growth of GaAs crystals. This method was

rejected due to problems explained below. Later, capping the samples with silicon nitride (Si_3N_4) proved to be a workable method.

2.511 Preliminary Testing Under Boron Oxide

To check the effectivness and feasibility of conducting deformation tests of GaAs under B_2O_3 in order to protect the GaAs specimen at high temperatures, a piece of a GaAs wafer and a small block of BN were placed in the bottom of a quartz crucible. The crucible was then filled with granular B_2O_3 and placed in the grower chamber. After sealing and pressurizing the chamber to 2kPa, the temperature was raised to 1000°C and held for 1200 seconds. Power was then removed from the heaters and the grower was allowed to cool.

Upon removal from the grower it was found that the quartz crucible had cracked. The BN piece did not appear to have been fully wetted by the B_2O_3. Recovery of the GaAs specimen was accomplished by dissolving the B_2O_3 in water. It was found that the B_2O_3 had adhered to both the BN and the GaAs. The small sample of GaAs was completely crumbled, presumably due to strains during solidification of the B_2O_3.

In a subsequent test a higher maximum temperature was reached and a more controlled, slower cooling rate was used.

The test was also arranged to apply a deforming load to the GaAs sample, Figure 13 shows the arrangement. Two rods of BN were machined to fit in the bottom of a small quartz boat. The test specimen of GaAs spanned these two support rods and a third BN rod was placed in the middle of the GaAs specimen. A stainless steel assembly of a bolt and two nuts was adjusted so that the two nuts fit over the edge of one end of the quartz boat and allowed the bolt head to swing down and rest on the top BN rod. This arrangement provided the deforming load to the GaAs. The boat was then packed with crystalline boron oxide and the whole assembly was placed in the bottom of the grower crucible. After sealing and pressurizing the chamber the temperature was raised to 600°C and held there for 300 seconds to allow the B_2O_3 to melt and cover the GaAs. The temperature was then raised to 1100°C and held for 1800 seconds. The chamber was then slowly cooled by leaving the heater power on automatic and lowering the set point 200C° at a time. This maintained an heater input of approximately 10 per cent of maximum throughout the cooling.

Again the quartz boat was found to have cracked. Recovery of the GaAs specimen was accomplished by dissolving the B_2O_3 in water. It was found that the B_2O_3 had adhered to both the BN and the GaAs. The BN rods were also found to be cracked. The small sample of GaAs had been broken into three larger pieces along with several finer pieces. The surface of the larger pieces of GaAs had been eroded quite severely. This procedure for

encapsulating the small samples of GaAs at high temperatures was considered unsatisfactory and thus rejected.

2.512 Silicon Nitride Capped Specimens

Another way of protecting the GaAs surface was to cap the surface with a protective layer which was inert to the GaAs and stable at high temperatures. Carbon was considered and rejected as it could contaminate the GaAs. Silicon nitride (Si_3N_4) was then considered as it is used as a cap for GaAs during electronic processing[8,9,10]. GaAs, capped with Si_3N_4, can withstand short anneals to 1080°C under static conditions. Silicon nitride does not contaminate GaAs. The Si_3N_4 cap is normally deposited by a vapour process to thicknesses from 500 to a few thousand angstroms. Damage to the GaAs surface due to the capping by this method is confined to the upper two hundred angstroms. In choosing the thickness of the cap, integrity of too thin a layer must be traded against cracking of too thick a layer. Typically, the thickness of Si_3N_4 used is 750 angstroms. For this work 750 to 800 angstrom thick caps were successful in protecting the GaAs surface. This thickness was also sufficiently thin to obtain CL images through the deposited layer since the excitation volume extends approximately one micron into the crystal, well beyond the Si_3N_4 layer.

Wafers of <100> grown GaAs were capped on both sides with a layer of Si_3N_4 750 to 800Å thick using a chemical vapour deposition process in Electrical Engineering, U.B.C.. The capped wafers were then cut into the specimens to be heated and deformed. All specimens were cut from the wafer with the long axis parallel to the major flat of the wafer, that is in the [011] direction. Figure 14 shows the orientation of the specimen with respect to the wafer. The width of each specimen was 6.35mm. Specimens for the static bending jig were cut to a length of 25.4mm. These were samples T1-5 from Cominco wafer J#44 and samples Si1 and L1 from Hewlett Packard wafers 273#45 and 293#9 respectively. Specimens for the dynamic bending jig were cut to a length of 32mm. These were specimens S1-4 from Cominco wafer 1214S61. The thicknesses of the wafers were measured as 0.40mm for J#44, 0.49mm for 1214S61, 0.48mm for 273#45, and 0.43mm for 293#9.

Wafer J#44 was a low grade wafer and was received in the as cut condition. It was first polished in a 15 per cent solution of bromine (Br) in methanol for 300 seconds to give it a mirror finish before capping. The two Hewlett Packard wafers had been previously etched lightly in molten KOH, and were cleaned in a 1:1:240 solution of NH_4OH:H_2O_2:deionized water (DI) before capping.

Individual specimens were identified with a specimen number printed onto the surface of one end with a diamond tipped scribe. With the labelled face up and the specimen number at the left end the middle half of each specimen was indicated by scribe marks place at the top left and bottom right corners of the centre region. These marks were used as references which would remain stable through heating and deformation. This middle region was then mapped by CL imaging through the Si_3N_4 cap before any treatment. A control piece from each wafer was also examined without a cap to compare with the CL images through the caps in order to assess the effect of capping on the CL emission.

2.52 Post Heating Specimen Treatment

After heating the specimens required polishing before CL imaging could be carried out. The process consisted of removing the Si_3N_4 cap in hydroflouric acid (HF), rinsing in deionized water (DI), and polishing in a 1:1:1 solution of NH_4OH:H_2O_2:DI. This is done to remove remnants left by the HF, of which there was an appreciable amount both in a visible form and in a surface film which prevents the normal polishing action of Br in methanol. Following this initial cleaning are rinses in deionized water and then methanol. Then, following the cleaning polish, a final chemical polish in a 5 per cent solution of Br in methanol was carried out followed by a methanol rinse.

Times for each step in the procedure depended strongly on the condition of the specimen. Each step of polishing was carried out while visually assessing the progress. When either a satisfactory surface was generated or no further improvement was obvious or if thinning of the specimen became a problem the polish was terminated. Typically, removal of the cap in HF was accomplished in 120 to 180 seconds with a water rinse for 180 to 300 seconds. The cleaning polish in the $NH_4OH:H_2O_2$:DI solution was normally conducted in two steps of 300 to 600 seconds each in fresh solution. The final chemical polishing using 5 per cent Br in methanol was also done in two batches of fresh solution with 600 seconds per bath. All cleaning and polishing was conducted at room temperature (20°C) with room temperature solutions. The cleaning and polishing solutions had to be fresh. A satisfactory surface was one with a mirror finish with as little remaining pitting as possible. At the very least the sharpness of the edges of any pitting had to be polished off.

2.6 Cathodoluminescence Imaging

2.61 Scanning Electron Microscope

The SEM has seven basic systems, a high voltage system to generate the beam of electrons, a vacuum system to provide the necessary vacuum to allow passage of a beam of electrons, a focussing and demagnification system to guide and focus the

electron beam onto the specimen surface, a scan system to raster the electron beam over a specific area of the specimen, a detection system to pick up the secondary electron (SE) signal generated by the interaction of the electron beam with the sample surface, a video system to display the detected signal coincident with the beam scan, and finally, a mechanical system for manipulating the specimen position and orientation within the vacuum chamber.

The beam is generated by applying an accelerating voltage (nominally 10, 20 or 30kV) to electrons that have been thermally emitted from a heated filament. This coarse beam is compressed by the electric field of the Wenhelt cap and is made to pass through a physical aperture (spray aperture) consisting of a precision hole in a metallic disc. The beam is further demagnified by a system of objective lenses before passing through the final aperture. Next the condenser lens is used to further demagnify the beam, while the focussing lens is used to set the point of minimum beam diameter at the surface of the specimen. Two sets of scan coils are used to raster the beam over the specimen surface. The signal generated by the beam's interaction with the specimen is picked up by the detection system and relayed to the video section which performs the raster on the cathode ray tube monitors synchronously with the beam. Magnification is the ratio of the video sweep to the beam sweep, and as the beam is made to raster over smaller and smaller

regions the magnification increases. Images from the SEM can be displayed on either (or both) of the two cathode ray tube monitors on the front panel. The right most screen is screen 1 and the image displayed on this screen is the same as the one that can be sent to the camera. The other screen, to the left is screen 2 and can be set up to display either the signal displayed on screen 1, some attribute of the image on screen 1 (brightness for example), or another signal entirely from the same specimen area as that displayed on screen 1. The most useful combinations are as follows:

1) SE image on screen 1 and brightness waveform on screen 2
2) SE image on screen 1 and CL image on screen 2
3) CL image on screen 1 and brightness waveform on screen 2

Combinations (1) and (3) are useful for adjusting the contrast and brightness for picture taking of either SE or CL images and also during the procedure of centring and saturating the filament. Configuration (2) is useful for simultaneously imaging the surface (SE image) of the specimen and the CL image for correlating particular features present in both images.

The whole of the electron system is maintained under vacuum. the filament which is heated to 'boil off' the electrons for the beam is similar to the filament in a light bulb. If there are any oxidizing elements present as gasses in the chamber this

filament will burn out very quickly. The filaments do burn out over time and their lifetime is greatly affected by how hot they are actually run. Beginning at low temperatures there are very few thermally excited electrons emitted, to increase the number emitted, that is to make the beam brighter, the temperature of the filament is increased. There is though a limit to this in that at a particular temperature there is no further increase in emission with an increase in temperature. At this point increasing the temperature only shortens the life of the filament. However, this is also the best point at which to operate since it gives the brightest beam. The procedure to accomplish this is referred to as saturating the filament and it is very important in terms of maximizing beam brightness without unnecessarily sacrificing the filament.

In order to achieve a sufficient electron beam current for CL imaging the filament must be centred and saturated under the conditions used for CL imaging. The procedure to accomplish this is as follows:

With a secondary electron image displayed on screen 1 select the single line scan mode and set the auto brightness to off. On the second screen choose the waveform mode and adjust the contrast and brightness controls to bring the scan intensity into the range of the screen. With that waveform displayed increase the filament current and monitor the height of the waveform on screen 2. Re-adjust the contrast and brightness as necessary to

keep the waveform on the screen. At saturation there will be no further increase in the height of the waveform (brightness) with an increase in the filament current.

If the filament is not centred there will, in fact, be a drop in brightness with an increase of filament current past saturation. To correct this condition the filament current is set in the over saturated range and the X, Y filament position adjustments are varied to maximize the brightness. Once this has been accomplished the filament current is again varied until the peak brightness condition is regained. The process of adjusting the filament current and centring the filament may require several iterations before the optimum conditions are found. Failure to obtain a satisfactory brightness (insufficient for CL imaging) after a few iterations usually indicate that the filament is too far off centre and it may have to be physically bent or even replaced. The high beam currents necessary for CL imaging were found to be detrimental to the filaments resulting in excessive warpage or in them becoming completely burnt through after about 20 hours.

The specimen to be examined in the SEM must be capable of dissipating any acquired charge by conduction and must be grounded to the SEM ground. If this is not the case then, over time, the specimen will pick up and store charge from the arriving beam electrons until this accumulated charge is

sufficiently large so as to affect either the incoming electron beam or the outgoing electron signal. This effect is known as "charging" and is detrimental to imaging of the desired signal.

The standard SEM detects the secondary electron signal generated from the specimen by the bombardment of the electron beam. This is only one of several signals generated. The incident high energy electron beam also generates an X-ray signal, a back scattered electron signal and the CL signal.

2.62 Cathodoluminescence Detection Equipment and Installation

A solid state CL detector was added to an ETEC SEM to obtain CL images. The detector, consisting of a four segment annular silicon diode with a high purity quartz window was attached with a brass clip bracket to the bottom of the SEM pole piece. The electrical connections to the detector passed through an optional port on the SEM used to house the mounting bracket and the electrical feed-through. The electron beam from the SEM passes through the central hole of the diode array in the detector and strikes the sample directly. A quartz window in the detector passes the CL signal but blocks the back scattered electron signal. The SE signal is still swept out by the Faraday cage of the SE detector and is available for normal SE imaging.

The CL detector signal is fed into a preamplifier which was installed immediately outside the port on the SEM used for the detectors electrical feed-through. The preamplifier receives the signal from the detector and passes it to the main amplifier. The preamplifier also provides each diode in the detector with the proper biasing and allows for zeroing of the detector. At the main amplifier each quadrant of the detector can be selected to be in either the on, off, or inverted mode. Brightness and contrast controls are also on the main amplifier. The amplifier output adds the signals selected and displays them on the video screen of the SEM.

2.63 Operating Procedure

In order to obtain CL images on the SEM, the instrument had to be set at the highest voltage available and the largest spot size had to be selected. Extra large apertures were required (890 or 1270 microns for the spray and 400 microns for the final). An indicated working distance of 25mm gave the best contrast. Grounding of the specimen was critical. The filament had to be centred and saturated before each session. The demands on the filament were high resulting in considerable shortening in the service life of the filament to only about 20 hours. The detector bias and zero had to be checked and reset following every ten sessions of CL imaging. Symptoms of an unbalanced condition included poor contrast or flooding in one quadrant of

the screen that could be improved by selectively turning off quadrants of the detector. Pictures of the CL images were most successful when taken in the 540 scan lines mode.

To begin a session the SEM must be on and in the auto mode (key above camera). The beam and filament must be turned off. The SEM chamber is vented (VENT button). The specimen, which is mounted on a stub with carbon dag is then put into the SEM chamber. The chamber door is then closed and held shut while simultaneously pressing the EVAC button. This will evacuate the chamber. The beam cannot be turned on until a vacuum level of 2×10^{-4} Torr is reached, however, delaying the turn on until the vacuum reaches 10^{-4} Torr helps to extend the filament life.

Once the beam is turned on a SE image is first used to locate the specimen and/or the area of interest. The initial imaging of the specimen and focussing are done with a small electron spot size (2.5-3.0 amps condenser current). The Z axis control and the coarse focus are used to bring the surface of the specimen into focus at an indicated working distance of 25mm (this corresponds with a magnification correction factor of 1.0). The spot size is then increased while simultaneously adjusting the focus controls to maintain the image. Once the largest spot size has been reached (1.6 amps condenser current), the Z axis control and the coarse focus are used to bring the specimen surface into focus at an indicated working distance of 25mm.

At this point the centring and saturation of the SEM filament should be checked and adjusted. If there is insufficient brightness to produce the initial SE image the centring and saturation procedure may be necessary for the small spot size (this is especially true immediately after replacing a filament). However, even if this is done, the centring and saturation must be checked and adjusted for the large spot size.

Next the CL mode is selected and displayed on screen two concurrently with the secondary image on screen one. The brightness and contrast controls on the CL main amplifier are adjusted to display the best CL image. A final focus and Z axis adjustment are required to bring the CL image into sharpest focus at an indicated working distance of 25mm.

The CL signal can be displayed in two modes; normal and inverted. In the normal mode areas that emit light in the detector's band width will appear bright on the SEM viewing screens. In the inverse mode the light emitting areas will appear dark.

2.7 Secondary Ion Mass Spectrometry Analysis

Some SIMS work was carried out in an attempt to explain some of the CL contrast effects in terms of impurities. This was accomplished by mapping areas of a crystal by CL imaging and then

comparing the concentrations of impurity elements between the CL bright and dark regions. Specimens of GaAs were mounted on specially adapted stubs that could be accommodated in both the SEM and the SIMS chambers. CL images were taken from several recognizable areas (adjacent edges and corners) for later reference for the SIMS imaging. The magnification used was 52× which gave the largest field in the SIMS. The mounted specimens were then transferred to the SIMS machine. Approximately 5000Å of surface material was eroded from the sample surface to remove contaminants. Then a series of spectrum sweeps were run to identify impurities present. Those found were mapped and their distribution was compared to the CL images. A direct comparison is made difficult since the SIMS map contains a degree of foreshortening as the specimen is inclined to the incident ion beam of the SIMS.

A similar study was conducted[7] and showed an increased concentration of Si, O, Cr, and C at the dislocation cell walls. The GaAs studied was not doped, the impurities were present only as residuals.

3 Observations

3.1 The Cathodoluminescence Process

The electron beam from the SEM generates an excitation volume in the GaAs which extends into the material in a tear drop shape to a depth of 2 to 3 microns. The incident beam spot, which is large to begin with, also spreads, reducing the resolution on the images. On the basis of measuring the minimum detectable separation of two distinct points in the image, the resolution is estimated to be 6 microns, which gives a useful magnification limit of 400 times. Most CL images were taken at a magnification of 32 times. For more detailed pictures magnifications of 64, 128, and 320 times were used. At the highest magnification loss of detail in the image is clearly apparent.

Specimen cleanliness is also critical as dirt, carbon dag (used for attachment and grounding of the specimen), and scratches appear clearly in the CL image, as dark regions. Images from dirt and scratches flared badly when using inverted imaging, reducing the overall quality of the image.

When a GaAs crystal is examined for CL two additional effects can occur. First, the high energy incident electron beam cracks the oil present in the vacuum atmosphere and leaves a

contaminating film of carbon on the specimen surface. This is not visible in secondary imaging but is sufficient to degrade the CL image over time. Secondly, light from the filament shines down through the large apertures in the SEM and illuminates the sample surface which affects the CL image. This is a persistent phenomenon which is only detectable on the CL image. The effect is most pronounced on clean, polished specimen surfaces and to a lesser extent on capped Si_3N_4 samples.

It was found that the observation time was limited to about two hours for each examination. During this period internal heating in the SEM was sufficient to increase resistance losses to the point that the high voltage producing the electron beam dropped too low for CL imaging. This was aggravated further by the low voltage of 27kV which was the actual voltage when the SEM was set at 30kV. In some sequences of CL micrographs a gradual loss of contrast will be apparent which is due to this progressive decrease of the high voltage with time.

3.2 Cathodoluminescence Imaging of GaAs

An inverted mode CL image of a section of a polished wafer of as-grown GaAs is shown in Figure 15. The image reveals a network of dark cell walls surrounding regions of little or no contrast. Since the image is inverted the dark features are

actually the more luminous. The contrast is due to local differences in CL emission around dislocation sites.

The cells (A and C) are predominantly featureless regions and vary in size from 300 to 1000 microns across. The cell walls (B) are darker overall than the cell interiors and contain groups, clusters and arrays of dark spots. In places the walls are only the width of a single spot, elsewhere the wall thicknesses increase to 100 microns and contain several spots across the width. These spots show the location and arrangement of grown in dislocations. These dislocations form into cell walls in the crystal during the growth process. In the interior of these cells are regions of relatively dislocation free material.

3.21 Cathodoluminescence Image compared to Etch Pits

After etching a piece of GaAs that had been mapped by CL it was found that the etch pits produced by molten potassium hydroxide (KOH), which are normally associated with dislocations at the surface, had an excellent correspondence to the spots and arrays of the CL images. This is evident by comparing Figure 16, an inverted CL image with Figure 17, an optical image of the same GaAs surface after etching in KOH. Cells marked A, B, and C as references are clearly evident in both figures as is the rest of the correspondence. The CL image, in Figure 16, displays a

clearer demarkation of the cell walls than in the case of the etch pits since dark regions surrounding the spots in the CL image serve to "connect the dots".

A similar comparison for a low dislocation density sample ($4\times10^3/cm^2$) is shown in Figures 18 and 19. There is excellent registration between the CL spots and the etch pits (A). Further, the CL image shows not only the location of the dislocations that result in etch pits but also regions around the pit sites that are lower in CL brightness. For a given group of pits in an area the etch pit pattern does not reflect the size or shape of the associated dark field around them in the CL image. This can be seen by comparing the two regions marked B and C in Figures 18 and 19. The dark regions around the dislocation sites in the CL image also make it easier to visualize the network structure of the dislocation arrays.

The CL image and the SE image (which indicates topographical features) are compared for a Si doped sample of GaAs in Figures 20 and 21. The etch pits, A, B, and C, produced by molten KOH, are seen as regular, hexagonal features in the SE image. The CL image shows the dark spots associated with the dislocations that correspond with these pits. Figure 22 shows the CL image of a Si doped GaAs crystal with a long dislocation evident as a dark line, running along the surface of the crystal. The KOH etched surface of the same area in Figure 23 does not

show any indication of this dislocation. In other areas of the same sample there were instances of dark spots appearing in the CL image but there was no corresponding etch pit visible in the SE image.

3.22 CL Contrast - Dots and Halos

The difference in CL intensity from various areas of the specimen can be attributed to several effects. When imaging a crystal of GaAs by CL, contrasting networks are easily resolved on the crystal. There was no corresponding feature visible in secondary electron image of the same area. This demonstrates that the networks imaged in CL are not a result of the topography of the specimen surface. In the first series of specimens the networks appeared bright on the CL image in the normal mode. This at first seemed to conflict with the notion that in the regions at and around dislocations CL emission should at least be shifted in wavelength out of the range of the detector if it existed at all, and thus they should appear dark.

Upon closer examination it was found that the bright spots that made up the arrays in the CL images were themselves made up of a dark central spot surrounded by a bright region. Figure 24 shows this in electronics grade GaAs (×128). At lower magnifications (×32) in the CL image of the same area, the dark core of the spots could no longer be resolved. A dislocation is

therefore imaged as a dark spot surrounded by a bright halo. This dot and halo effect has been reported by other workers[7,10,11,12]. It has been proposed that the effect is caused by the distribution of impurities around the dislocation. The dislocation itself is a site of non-radiative recombination, hence a dark spot. However, the dislocation may also act as an impurity sink. Impurities would diffuse from the region around the dislocation to the dislocation core, thus generating a region around the dislocation lower in impurities than the bulk crystal. The impurities give rise to recombination at wavelengths different to those of the pure crystal. These new wavelengths may be outside the detection limits of the CL detector in the SEM. This would make regions of higher impurity concentrations appear darker, giving a dark spot, and regions swept clear of impurities brighter, accounting for the halo. From the proposed mechanism it is not clear which plays the greater role in generating the dark spot, the dislocation itself or the cloud of impurities it has gathered.

Regardless of the mechanism resulting in the contrast in the CL images, the apparent dislocation networks imaged by CL corresponded well with KOH etch pits produced on the same surface. The CL images of the dislocations appear as either light or dark, depending upon the crystal and its history. In most cases the best images were obtained when the detector mode was chosen to display the networks as dark regions. As a result,

the imaging mode which shows the dislocation arrays as dark is generally used. A conscious effort is thus required to mentally invert the contrast in the inverted CL images before drawing any conclusions on the nature of the impurity distribution.

3.23 Surface condition

In the early part of this investigation low grade GaAs wafers with as-cut surfaces were examined. The cut surfaces were smooth but not with a mirror finish, the surface appearing matted. These surfaces could not be imaged by CL; only large topographical features could be detected. After polishing these samples in a 15 per cent solution of Br in methanol for 600 seconds the surface had a mirror finish which was suitable for CL imaging.

3.24 Gallium Arsenide Capped with Silicon Nitride

To determine whether the Si_3N_4 capping of the GaAs influenced the CL image, and whether an image could be obtained through the layer, two pieces of the same crystal were examined by CL imaging, one without capping and the other with a Si_3N_4 cap 750Å thick. The results showed that the dislocation arrays were clearly visible which indicated that any surface damage due to capping did not affect the dislocation image. There was a small amount of added contrast in the CL images of the capped samples,

appearing as a slight mottling. This may have been due to both the damage in the GaAs as well as the actual layer of Si_3N_4.

3.25 Secondary Ion Mass Spectrometry Analysis

The bright and dark regions in the CL images are possibly associated with differences in impurity levels, the bright regions being associated with depleted regions. This has previously been investigated[5] using SIMS. The concentration of impurities would be very low, on the order of $10^{15}/cm^3$, that is at the residual level. Attempts were made to determine whether the bright regions were impurity depleted using secondary ion mass spectrometry (SIMS).

A GaAs sample was examined after heating for 1200 seconds at 1000°C. CL images at two magnifications are shown in Figures 25 and 26. The bright ring marked A in the figures is due to a surface defect. A SIMS map of the same surface area after 5000Å had been removed is shown in Figure 27. This map shows the distribution specifically of carbon. The large bright circle corresponds to the surface defect at A. Comparing Figure 26 with 27 (B, C marked for reference) indicates that some correlation exists between the dark regions in the CL image, associated with dislocations, and the bright regions in the SIMS image associated with higher carbon levels.

A direct comparison is made difficult since in the SIMS the specimen is inclined to the incident ion beam whereas in the SEM the CL image is taken with the specimen surface normal to the incident beam. This results in the SIMS image containing a degree of foreshortening relative to the CL image.

3.3 Heated Specimens

Samples of GaAs were capped with 750 Angstroms of Si_3N_4. To the naked eye the capped samples appeared as a blue, mirrored surface (the colour is used as an indication of the thickness of the Si_3N_4 layer : 700-800Å appears blue). The SE image in Figure 28 shows the topography of the capped surface at a magnification of 200 times. The surface is quite bumpy relative to the clean GaAs surface.

The capped samples were placed in a crystal grower and heated to approximately 950°C, held at temperature for 120 seconds and slowly cooled. Figure 29 is a SE image of the surface after heating. The cap is still in place, but there are numerous pinholes in it. The CL image from the area in Figure 29 is shown in Figure 30. The damage features in the cap are observed to be most prominent in the image, overshadowing the underlying dislocation structure.

The remainder of the cap was removed in HF and upon further examination it was found that pits had developed in the GaAs surface under the cap pinholes. These were estimated to be half a micron deep from optical and SE images. Attempts to image the CL signal from the GaAs after removal of the cap were unsuccessful as the pits themselves were the prominent feature. It was not until much of the pitting damage was polished off that the CL signal of the underlying dislocation structure could be imaged.

The effects of heating GaAs on the CL image were determined by examining sample T4 which was heated to 955°C for 360 seconds, then cleaned and polished. Figures 31 through 34 are CL images (×32) of areas of sample T4. The CL images in Figures 32 and 34 are from adjacent areas of the specimen after heating, taken in the normal imaging mode. The dislocation arrays appear dark and the images are quite sharp. This is compared against the CL images in Figures 31 and 33 taken from the same areas of the specimen before heating. These were taken in the inverted imaging mode. Hence the arrays actually appeared bright in the CL image before heating.

The arrangement of the dislocation networks remain essentially the same, with minor deviations after the heating. There is a contrast inversion after heating and there is an increase in clarity or sharpness of the CL image after heating.

A sample of the same specimen which had been capped, but not heated, was put through the same cap removal, cleaning and polishing procedures as the heated portion to determine if any of the observed effects could be attributable to specimen treatment after heating. Subsequent CL imaging of this sample gave the same fuzzy inverted image obtained from the capped sample before heating. This indicates that the contrast inversion and sharpening of the CL image are a result of the heating and are not due to the polishing procedure.

A comparison was made of CL total brightness before and after heating. This was done by examining two specimens mounted on the same specimen stub. One specimen was as supplied and the second had been heated to 1000°C. The CL images of both samples had roughly the same overall brightness. Moving from one specimen to the other did not require any brightness adjustment to keep the signal level constant.

3.4 Static Bend Specimens

Specimens T1, T2, T3, T5, Si1, and L1 were all bent in the static bend jig shown in Figure 9. After placing each test assembly in the grower chamber, the temperature was slowly increased. Specimens T1 and T2 were tested simultaneously, as were T3, Si1, and, L1. Specimen T4 was tested with T5 but was

only heated, not stressed. The deforming load in each case was 12 grams (0.118N), applied at the free end of the specimen 14mm from the bearing support.

Specimens T1 and T2 deformed at approximately 950°C. After bending, the temperature was held constant for 120 seconds before cooling. The centre deflection, limited by the jigs guides, was 0.2mm for each specimen . Figures 35 through 38 are a series of CL images taken of specimen T2 after heating, bending, subsequent removal of the cap, cleaning, and polishing the sample surface. The sequence covers the specimen from near the free end (Figure 35) where the applied bending moment is minimal, to near the bend axis (Figure 38), where the applied bending moment is a maximum. The CL images between are of increasing proximity to the bend axis (increasing applied moment). The images were taken in the normal mode at a magnification of 128 times.

The dark circular regions that appear in some of the images are those persistent apparitions described as side effects earlier in the CL imaging section. These dark circle were not immediately apparent whenever a new area of the specimen was brought into view during CL imaging. After each region was brought into focus and contrast and brightness levels were set for photographing, these circular features began to develop. As the time spent imaging a particular area increased, the circle in the field grew darker. Usually the time needed for the

photographic scan was sufficient for these circles to develop from unnoticeable to the level in the CL images shown.

The dislocation arrangement in this series of CL images is different from the as-grown cellular structure as seen in Figures 31-34 taken from the same wafer. In the sequence of CL images of specimen T2, the dislocations image as dark spots or lines with no halos. The dislocations are no longer found in their original cellular structure but have formed into arrays parallel to the bend axis. Between these arrays are areas substantially clear of dislocations. The spacing between the arrays decreases nearer the bend axis.

Figure 35 was taken near the free end of the specimen 12.5mm from the bend axis. The alignment here is minimal, and parts of the old cellular structure are still visible. Figure 36 was taken at 7.5mm from the bend axis. The alignment of dislocations here is quite clear with the appearance of short line segments along with the aligned single spots. The CL image in Figure 37 was taken at 3mm from the bend axis. The density of dislocations is increased from the previous figure and there are more dark line segments present. Finally, Figure 38 was taken at 1.5mm from the bend axis. Again the dislocation density has increased over the previous figures. There are more, longer, dark lines present in this region.

The densities of the new arrays in this specimen measured 2, 22, 40, and 53 lines per mm at 12.5, 7.5, 3, and 1.5 mm from the bend axis.

Sample T5 was bent at 955°C and was left at temperature for 360 seconds following the deformation. The centre deflection achieved by sample T5 was measured as 1.0mm. The same uncapping and polishing procedures were applied before taking the CL images shown in Figures 39 to 42. The dislocations again appear as dark lines or spots with no halos.

Figures 39 and 40 are CL images (×32 and ×128 respectively) taken from the high strain region of specimen T5 near the bend axis. The applied bending moment is highest in this region. The image in Figure 39 shows a very fine matte pattern of dislocations, with no remnant of the as-grown dislocation arrays present. At higher magnification of the same area, Figure 40 resolves the dislocations into arrays. These arrays have linear features parallel to the bend axis. These new arrays have a density of 70 lines per mm in this region.

Figures 41 and 42 are CL images (×32 and ×128 respectively) taken from the low strain region of specimen T5 nearer the free end. The applied bending moment is lower in this region. In Figure 41 the old network patterns of the as-grown dislocations are still visible. Superimposed on this however, are many fine

lines parallel to the bend axis. The higher magnification image in Figure 42 clearly resolves the new linear dislocation arrays with wider spacing and lower density than those in Figure 41.

Specimens L1, Si1, and T3 were tested simultaneously in a slowly increasing temperature environment. They started deforming at close to 950°C, with bending starting at different times for the three specimens. The low dislocation density specimen L1 was observed to deform first, at the lowest ambient temperature, followed by T3 and finally the Si doped specimen Si1. The temperature differences between the onset of deformation of the three specimens were not established but small.

The CL images (×128) shown in Figures 43 and 44 were taken from regions of specimen Si1 after bending. Figure 43 was taken nearer the free end in the low strain region. Visible are three (A, B, and C in the figure) of the as-grown dislocations (compare with Figure 20). Also present are linear arrays of dislocations made up of either long single lines or a series of short segments each parallel to the bend axis. The new arrays lines are very much sharper than the original dislocation images.

Figure 44 was taken from the region of Si1 nearer the bend axis in the high strain region of the specimen. New arrays of dislocations are seen as fine dark lines and spots arranged

parallel to the bend axis. There is a higher density of these new arrays than in the low strain region of Figure 43, and no evidence of as-grown dislocations is present.

The top and bottom surfaces of deformed specimen T3 were examined to compare the dislocation configuration on the tension and compression sides of the specimen. CL images showed the dislocation pattern was the same on both sides, and was similar to that shown in Figures 35 to 38, with arrays of new dislocations parallel to the bend axis.

3.5 Cyclic Bend Specimens

The bending experiments described above established the temperatures at which plastic deformation occurred in GaAs and the extent of generation of new dislocations with strain. On the basis of this information a more systematic series of bending tests were carried out in which small cyclic strains were applied to the specimen using the apparatus shown in Figure 10. For this series of tests, specimens 32mm long and 6.35mm wide were used, cut parallel to the major flat from an electronics grade GaAs wafer. This is the same orientation as used in the static tests and shown in Figure 14. Prior to cutting, the wafer was capped with 800Å of Si_3N_4 which was removed after deformation.

For specimen S1 the maximum centre deflection was set at 0.5mm, with a strain rate of 0.21mm/s. The test temperature used was 1000°C. The specimen was cycled five times with a 30 second pause at each end of travel.

Figures 45 and 46 are CL images (×32 and ×128 respectively) taken from the high strain region of specimen S1 near the bend axis. The applied bending moment is highest in this region. A mixture of linear arrays parallel to the bend axis and fine cellular networks are just visible in Figure 45. These become clearly resolved in the higher magnification image in Figure 46 from the same area. The cell size of the new dislocation networks is approximately 30 microns, much smaller than the as-grown cell size of 500 microns. Long arrays of dislocations parallel to the bend axis are also evident.

A CL image (×32) of the low strain region of specimen S1 is shown in Figure 47. Here the boundaries of the as-grown dislocation arrays are still visible, but lack clarity. Figure 48 is a CL image (×128) showing region A from Figure 47 at higher magnification. The new dislocation density is higher than before the bending, but the distribution is more homogeneous with no strong cellular or linear alignment. There appears to be no relation between new dislocations and the old network boundaries (the darker areas).

In the second cyclic test with specimen S2, the maximum deflection was also 0.5mm, with a strain rate of 0.21mm/s. The test temperature was increased to 1050°C, and S2 was cycled four times with a 120 second pause at each end of travel.

The higher temperature caused a decomposition and melting of the specimen ends. The centre region of the specimen remained intact, but the test clearly established the upper temperature limit for the present series of experiments.

A CL image (×128) of specimen S2 from the high strain region near the bend axis is shown in Figure 49. As before, a high density of dislocations has been generated, similar to S1, with linear arrays parallel to the bend axis and a fine cellular array structure.

For sample S3 the maximum centre deflection was reduced to 0.25mm, and the strain rate to 0.014mm/s. The test temperature was returned to 1000°C. S3 was cycled only once and allowed to anneal for 90 seconds at the end of the cycle. The thermal history for S3 is shown in Figure 50. The heating and cooling rates shown are representative of all tests.

The effect of high temperature deformation on specimen S3 in a low strain region 6mm from the bend axis is shown in Figures 51 and 53. These are CL images (×128) of the same area of the

specimen before and after deforming respectively. The tangle of dislocations at "A" shows some realignment, but is recognizable. The rest of the new dislocation structure in Figure 52 cannot be directly related to the dislocations in Figure 51.

CL (×32) maps of the middle 12mm of specimen S3 before and after deforming are shown in Figures 53 and 54 respectively (covers two pages). The image in Figure 53 was taken in the inverted mode. The maximum strain took place at the centre, (A - A).

The as-grown cellular boundary structure (examples B and C) at the low strain ends of the specimen are clearly evident after high temperature deformation. However, there has been a considerable change in the CL image of these cells. Cell C in Figure 53 is shown with a bright interior and the boundary consists of grayed region containing dark spots. The image was taken in the inverted mode though and therefore, the cell interior is darker than the boundary and the dislocations appear bright. In Figure 54 the interior of cell C is bright, the boundary is dark and the dislocations appear as bright spots in the boundary. There is not an exact correspondence between the dislocation spots in the cell boundaries before and after the deformation.

Upon approaching the centre, higher strain region in Figure 54, the occurrence of the bright dislocation spots in the as-grown cell boundaries diminishes and the boundaries themselves lose clarity. A finer network of dislocation lines becomes apparent. These new arrays are arranged parallel to the bend axis.

The test conditions for specimen S4 were kept as those for S3 except that S4 was cycled three times with a 120 second pause at each end of travel. The specimen was cleaned and polished as before and examined.

In the centre region arrays of new dislocations had formed parallel to the bend axis. These appeared as fine dark lines and spots and were most dense in the highest strain region. The as-grown cell boundaries were still visible but only as slightly greyer regions with no clarity or detail. In the low strain region the CL image was overall much darker than in the high strain region. Here the as-grown boundaries appeared as dark regions containing bright spots, as in the case of the low strain region of S3. Separating these two regions was an exceedingly sharp transition. The brightness of the CL image changed markedly over the transition and the bright spots in the as-grown cell boundaries, visible up to the transition in the low strain region, were not present upon crossing into the high strain region.

A sequence of CL images (×128) was recorded beginning at the centre, highest strain region, of the sample and proceeding toward the low strain region. Figures 55 through 59 show the new dislocation distribution in the high strain region. Figure 55 was taken at the bend axis. The new dislocation arrays, made up of long linear structures and spots, are aligned parallel to the bend axis and are closely spaced. In Figure 56, taken adjacent the area of Figure 55, the same type of arrays appear with a slightly greater spacing and with more instances of shorter line segments making up the arrays. Further away from the bend axis in Figure 57 the alignment of the new arrays is still apparent, but the arrays consist more of short linear segments and dots. The spacing between the arrays is also increased. Further away still from the bend axis the dislocation arrangement is shown in Figure 58. Here the arrays contain only short segments and spots. The long linear features visible in the higher strain regions no longer appear. There is still alignment of the new arrays parallel to the bend axis. Finally, Figure 59 shows the dislocation arrangement near the transition to the low strain region. The appearance of even short linear segments has diminished here with the majority of the dislocations appearing as spots. The dislocation density is at a minimum for the high strain region and the dislocations do not show a strong alignment. The slightly greyer regions in the image are remnants of the as-grown cell boundaries.

The transition from the high strain (bright) region to the low strain (dark) region is shown in Figure 60. The width of the transition is approximately 20 microns. The darker outer regions (one to either side of the centre bright region) are symmetrical about the centre region and the centre loading pin. Each dark region intersects the centre region with a parabolic profile extending furthest along the centerline of the specimen. Separation of the two dark zones was 9mm along the central axis of the specimen.

Figure 61 shows the CL image (×128) of the dislocation arrays in the low strain region just beyond the transition. The dislocations image as bright spots and are predominantly arranged in the as-grown cell boundaries. This is in contrast to Figure 59 which was taken approximately 2mm closer to the centre.

4 Discussion

4.1 Cathodoluminescence Imaging

Dislocations in GaAs are clearly delineated in the CL image provided the surface is well polished. The CL image of a dislocation consisted of a dark core sometimes surrounded by a bright halo. Where the halo was present it was sometimes sufficient to obscure the dark core, particularly at lower magnifications. In these cases the dislocations appeared as bright spots. There is excellent correlation between the dislocation spots in the CL image and dislocation revealing etch pits introduced by etching the GaAs in molten KOH. The CL image also contained additional grey level contrast that outlined the as-grown cell boundaries, which made the cellular structure more apparent than the etch pit pattern.

Heating the GaAs to 950°C served to enhance the CL image. The halos around the dislocation sites disappeared revealing the dark cores. The image was much sharper after heating. The dislocation arrangement was not significantly affected by heating alone and CL images taken after heating showed general correspondence with the features present before heating.

4.2 Deformation

The grown-in dislocation arrangement of networks could be affected by straining the crystal at high temperatures. The amount of change in the dislocation distribution depended upon the amount of strain and on the amount of energy (cycles) put into the crystal. At low strains, only minor re-arrangement was accomplished. At high strains, complete obliteration of the original arrays was possible at the expense of a far more dense distribution of new arrays. Between these two extremes was found the realm of just being able to remove the old arrays and replace them with a series of new arrays formed parallel to the bend axis with dislocation free regions between them. The spacing between these new arrays varied with the amount of strain introduced. At the limits approaching that of reducing the strain to levels that did not affect the original arrays the new dislocations were at low densities and did not exhibit strong alignment. The transition (yielded to non-yielded) occurred over a very narrow region, 20 microns wide, and it was immediately inside this yielded zone that the old arrays disappeared and the new dislocations were present at their lowest density.

4.21 Formation of Linear Arrays

GaAs has its slip systems on {111}<110>. In the present specimen orientation, slip can only take place on two of these

{111} planes, both are shown in relation to the specimen in Figure 62. The bend axis is along [01$\bar{1}$]. Both these slip planes, (111) and (1$\bar{1}\bar{1}$), intersect the specimen surface at right angles to the specimen length, or parallel to the bend axis. Dislocations in the crystal can glide to the surface on these two slip planes. Not every slip plane is expected to operate, instead, slip is more likely to occur on several parallel slip planes separated by regions which do not slip. As more deformation is required, more slip planes will come into operation. The resulting arrays seen on the surface are then also parallel to the bend axis with a spacing representative of the inverse of the amount of deflection (curvature) achieved.

4.22 New Array Density

The density (inverse spacing) of the new arrays formed parallel to the bend axis in the statically bent specimens (T1,T2,T5) was found to vary nonlinearly with the distance from the bend axis. The bending moment applied to the specimen varies linearly from a maximum at the bend axis to a minimum of zero at the applied load. The variation of strain at the specimen surface is not expected to vary linearly though since the elastic core diminishes while approaching the bend axis beyond the onset of surface yielding. The strain at the interface between yielded and elastic region will be roughly constant and is given by the yield stress divided by the elastic modulus for that temperature.

Following the assumption that planes initially perpendicular to the neutral axis remain planar after the deformation, the strain in the sample varies linearly with the distance from the neutral axis. Therefore, the deeper the yielded depth, the deeper will be the constant value of strain at the interface and the greater the surface strain will be. This can be seen by the construction in Figure 63. There will also be a degree of uncontrolled strain at the bend axis due to the formation of a plastic hinge (increasing strain does not increase stress). This is a limiting approximation but stress strain curves for GaAs[2] show a flattening stress strain curve above yielding at increasing temperatures, Figure 2.

Table II shows the new dislocation line densities and associated moment arm and applied load for specimen T2. In Figure 64 the data of table II has been plotted along with a parametric curve of surface strain versus distance from the bend axis developed from the arguments above. There is a good fit between the dislocation line density data and the form of the parametric curve, which is scaled appropriately.

If the Burgers vector of the dislocations is taken as $b = \frac{a}{2}[1\bar{1}0]$[1,3], then the displacement along the surface of the specimen, parallel to [011] is $\frac{a}{2}$ per dislocation. With the scaling factor (roughly 40 lines/mm corresponds to an $E\epsilon$ of 8MPa) from the above fit, and a room temperature value for the modulus

each line seen in the CL image would correspond to some 20 dislocations. It is expected however, that the modulus for GaAs at 1000°C is considerably reduced from the room temperature value. It is also reasonable to assume that the dark lines in the CL images do contain more than a single dislocation. The resolution available is well below that needed to disprove this and TEM work[1] showed that a single line of etch pits found in deformed material corresponded to arrangements of several closely spaced dislocation loops.

dislocation line frequency (lines/mm)	moment arm (mm)
~2	1.5
22	7.5
40	11
53	12.5
applied load = 12g centre deflection = 0.2mm	

TABLE II. Density of linear arrays along specimen.

The degree of "uncontrolled strain" is only uncontrolled with respect to the specimen itself. The bending apparatus used here provide an external limit to the absolute amount of bending. In specimen T5 where the centre deflection was increased to 1.0mm the new array density near the bend axis was increased to 70 lines/mm.

4.23 Yield strength

A simple plastic hinge theory[13] gives a yield point for the specimens in the static 3-point bending apparatus. Since the specimens exhibit plastic bending at a specified temperature under a known moment, the resisting moment (M_{resist}) in the specimen at that temperature could no longer increase and therefore, the specimen can be assumed to be behaving plastically at a roughly constant yield stress, YS. The resulting stress distribution generates a couple about the bend axis, equal to M_{resist}. With a specimen of width w and thickness t, M_{resist} is given by

$$M_{resist} = \frac{YS \cdot w \cdot t^2}{4} \qquad (1)$$

This value is then equated to the bending moment applied to the specimen (load × moment arm) and a yield stress at the bending temperature determined. For T1, T2, and T5 this was found to be 6.5 MPa at 955°C. This compares very well with the monotonic decrease of yield strength versus temperature[2] for 250-550°C. Figure 65 shows the data plotted along with an expected value of zero yield strength at the melting temperature. The comparison between yield strength values in compression tests along <100>[2] and bending about the [01$\bar{1}$] axis is valid since the Schmid factors required to resolve the stress onto the slip planes are the same, 0.408, for each system. Based on the above

value for yield stress the critical resolved shear stress (CRSS) for GaAs at 955°C is calculated as 2.65MPa.

The assumption that the whole of the specimen yields is reasonable, since even if an elastic core remained in the specimen, its contribution to the resisting moment would be small owing to the short moment arm such a core would have about the neutral axis. In effect, if a 50% elastic core remained 92% of the resisting moment would be generated from the yielded region.

4.24 Calculation of Parameters from Cyclic Tests

In the case of sample S4 there seemed to be a well defined yielded zone, that is the brighter centre region. The whole specimen was in the same thermal environment and there were no features on the bending jig that could be associated with the change. The only variable changing along the axis of the specimen was the magnitude of the applied bending moment. The profile of the zone was characteristic of yielding taking place under plane strain/plane stress conditions from the middle of the sample to the edges[14]. An estimate of the actual load applied to the specimen was calculated based on the width of this zone, the geometry of the bending jig, and the estimate of yield strength arrived at from the preliminary tests. The construction in Figure 66 shows a crystal of thickness t and width w, consisting of an elastic core surrounded by a yielded layer of depth YD,

with yield strength YS. The resisting moment is given by

$$M_{resist} = \frac{YS \cdot w}{3}\left(-YD^2 + YD \cdot t + \frac{t^2}{2} \right) \qquad (2)$$

The applied moment is given by

$$M_{applied} = \frac{P}{2}\left(\frac{L}{2} - x\right) \qquad (3)$$

Where the crystal changes from the yielded bright region to the elastic dark region the yield depth, YD, goes to zero. Equating the applied and resisting moments at this position gives an expression for the applied load P.

$$P = \frac{YS \cdot w \cdot t^2}{3\left(\frac{L}{2} - x\right)} \qquad (4)$$

The result for P was 0.338N (34.5 grams). A value of 5.45MPa was used for YS. This was an extrapolated value between 6.5MPa found at 955°C and zero expected at 1238°C, the melting point. With this calculated value for the applied load it was possible to find if the centre of the specimen did go fully plastic and how wide a zone about the centre loading pin was fully yielded. This was accomplished by setting YD equal to half the specimen thickness in equation (2) and solving for x. The result was that full yielding took place out to an x value of 0.4mm, or that

there was a fully yielded zone 0.8mm wide about the centre loading pin. This is consistent with the assumption made in arriving at the original value of the yield stress.

A final calculation was made to provide internal consistency with the above calculations and assumptions, and this was for the generation volume depth of the CL signal. Following the construction in Figure 67, the transition width between the yielded and non-yielded zones in the CL images is related to the depth of the signal generation volume and the rate of change of depth of the yielded region, dYD/dx, at x equal to 4.5mm. Differentiation of equation (2) and substituting 4.5mm for x gave the slope of the interface (0.03mm/mm). The transition width was measured from a 128 times CL photograph and was found to be 20 microns. This gave a CL generation volume depth of 0.6 microns. It has been previously reported[15] that the CL signal depth is one third of the electron beam penetration depth. Based on the above, the electron depth in this work is estimated to be about 2 microns. This is a reasonable value for the penetration of 27keV electrons into GaAs.

4.25 Estimation of Parameters To Move Dislocations

A load of 0.118N was applied to the free end of specimen T2, 14mm from the bend axis. In specimen T2 significant rearrangement of dislocations into linear arrays parallel to the bend axis was

accomplished 7.5mm from the bend axis. The bending moment at this point is calculated from equation (3) realizing that 0.118N is $\frac{P}{2}$. Assuming that this region is outside the zone where surface yielding takes place the surface stress can be calculated from the flexure formula below.

$$M = \frac{\sigma \cdot I}{c} \qquad (5)$$

At the surface c is half the thickness and I is the moment of area about the neutral axis. The calculated value for surface stress is 4.5MPa, which is below the calculated yield stress, validating the assumption. The resolved shear stress to achieve this dislocation arrangement is 1.8MPa at 955°C.

Similarly, for specimen S3 at 6mm from the bend axis a tangle of dislocations was basically preserved through the deformation as were the outlines of the as-grown cell boundaries at this position. Most of the dislocations though had been moved within the boundaries. The conditions of loading applied to the this specimen were the same as for S4 (cycles and times were different) so the value of 0.338N calculated as the centre deforming load for S4 can be assumed to have been applied to S3. The resulting surface stress from equations (3) and (5) is 4.5MPa, and the resolved shear stress is 1.8MPa.

In specimen S4 there was a clear transition between low strain regions where the as-grown networks survived to the high strain region where only the new arrays of dislocations were present. The boundary was assumed be where the surface just reached the yield stress, which was estimated to be 5.5MPa at 1000°C. The resolved shear stress value is then 2.2MPa. However, S4 was not subjected to a single cycle of loading and the resulting development of the sharp transition may be more controlled by the amount of thermal and mechanical energy introduced over the cycles.

To estimate strains that follow from the above stress levels requires a value for the modulus near 1000°C. It is clear from common sense and the results in section 4.22 above that the modulus at this temperature is between the room temperature value and some lower limit. A good value was not established, but using a value half that of the room temperature value translates the above stress levels to strains of approximately 0.3 microstrain. The radius of curvature to produce this strain level for the given specimens is approximately 800mm.

4.3 Conclusions

1) The as-grown dislocations in GaAs are moved with the application of strain at high temperatures. Resolved shear

stress levels needed are between 1.8 and 2.2 MPa in the temperature range of 950 to 1000°C.

2) Annealing alone to 955°C does not significantly affect the arrangement of the as-grown dislocations, but does affect the CL image, inverting the contrast and improving the clarity.

3) Bending of GaAs single crystals leads to the formation of linear dislocation arrays along the intersection of {111} slip planes with the specimen surface. The density of these new arrays varies with the amount of strain.

4) At 955±10°C GaAs has a yield strength of 6.5MPa along <011> and a corresponding CRSS value of 2.65MPa.

5) CL imaging can be used to characterize GaAs with respect to the arrangement of dislocations.

6) Si_3N_4 is useful as a protective cap for GaAs for temperatures under 1050°C.

5 Future Recommendations

Future work in this area can extend on three fronts :

1: Improvements in CL imaging, including better resolution by increasing the beam current by means of a more sophisticated filament (pointed or LaB_6), and increasing the accelerating voltage by modifying the SEM, both of which would allow the use of a smaller electron spot size.

2: More controlled deformation of GaAs samples using constant curvature jigs with parameters gained from this work to generate larger regions of crystals with uniform distribution of dislocations for studies on electrical properties.

3: Interdisciplinary studies on GaAs between Electrical and Metallurgical engineering including CL studies of failed devices, electrical properties of deformed GaAs, and use of CL to correlate device performance with dislocation distribution. This last point was discussed and would involve CL mapping of a region of a GaAs wafer prior to fabricating an array of identical devices on the wafer. Subsequent performance of the individual devices could then be compared with the underlying dislocation structure.

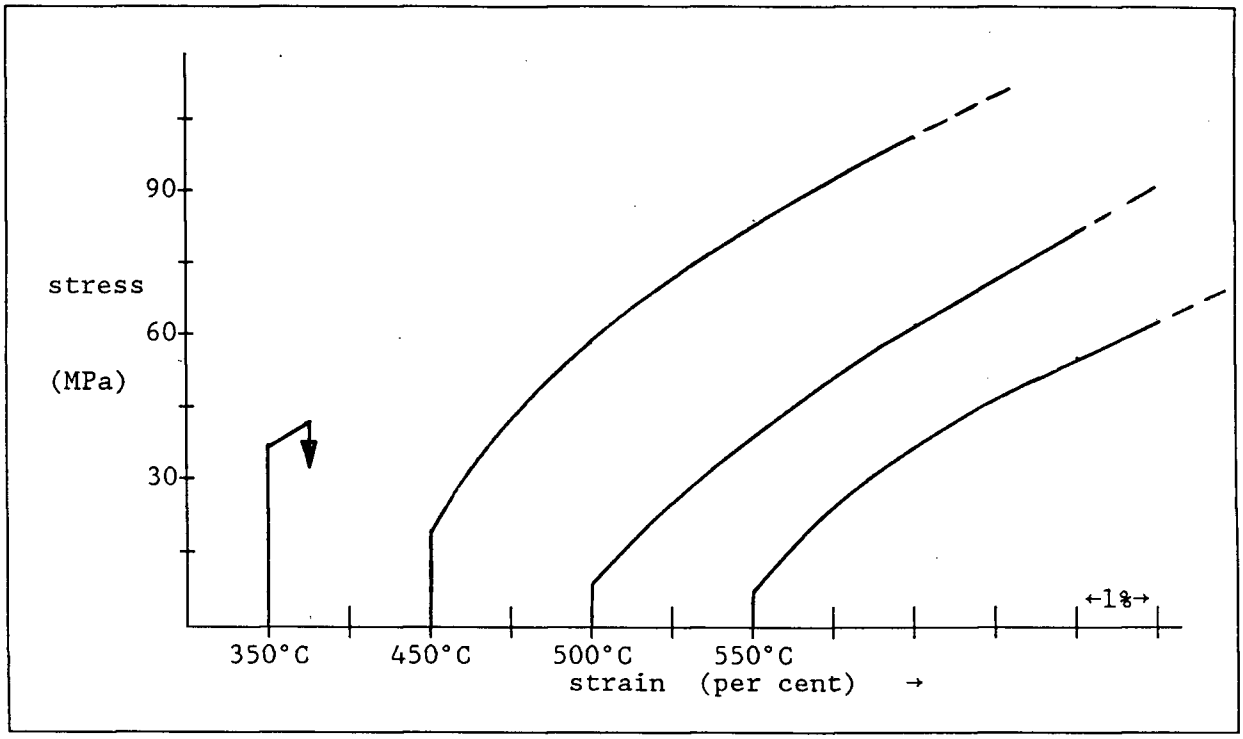

FIGURE 1. Stress versus strain for Si doped GaAs at various temperatures, tested in compression along <100> axis[2].

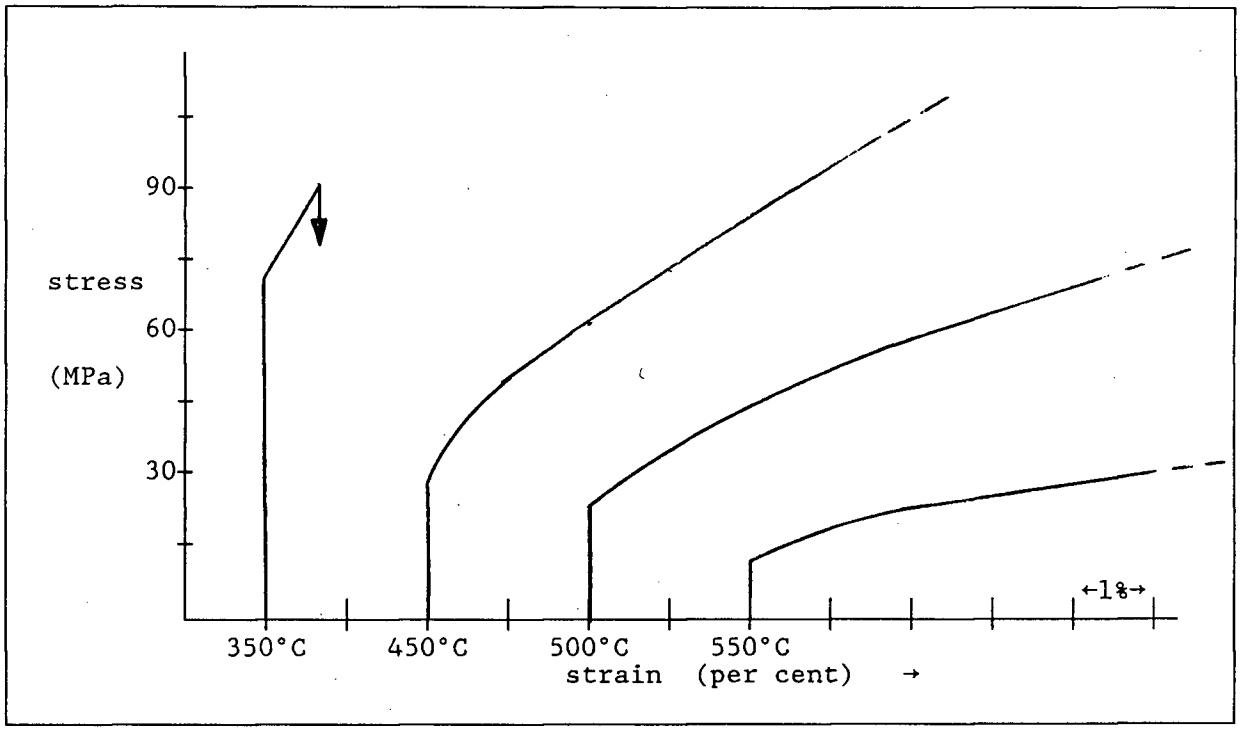

FIGURE 2. Stress versus strain for Si doped GaAs at various temperatures, tested in compression along <111> axis[2].

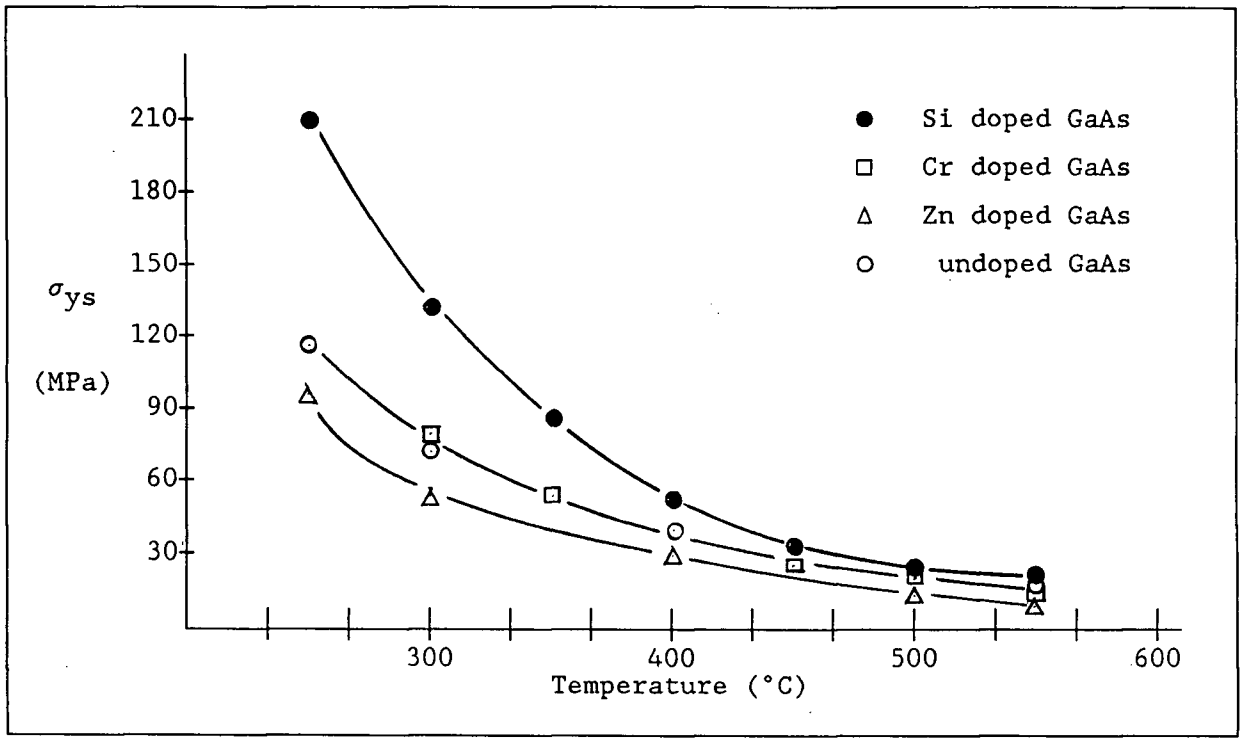

FIGURE 3. Yield stress versus temperature for various samples of doped GaAs tested in compression along <100> axis[2].

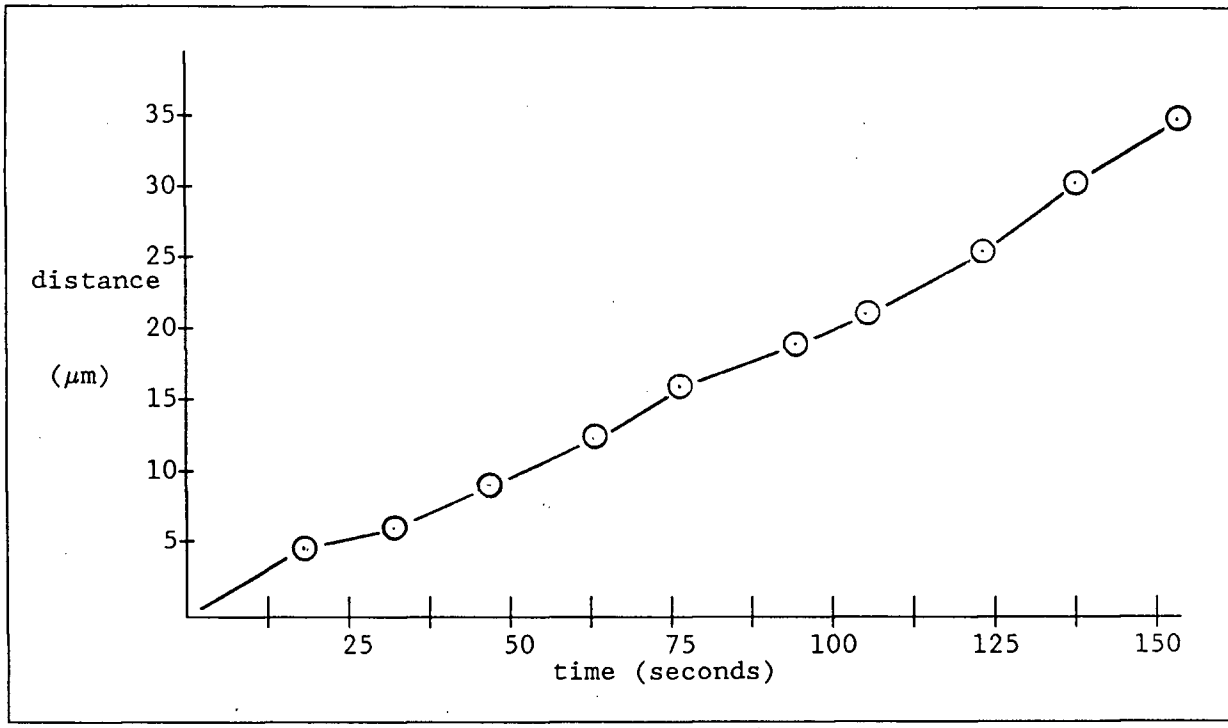

FIGURE 4. Dislocation position versus time from CL image of GaAs under an applied stress of 47MPa at 195°C[3].

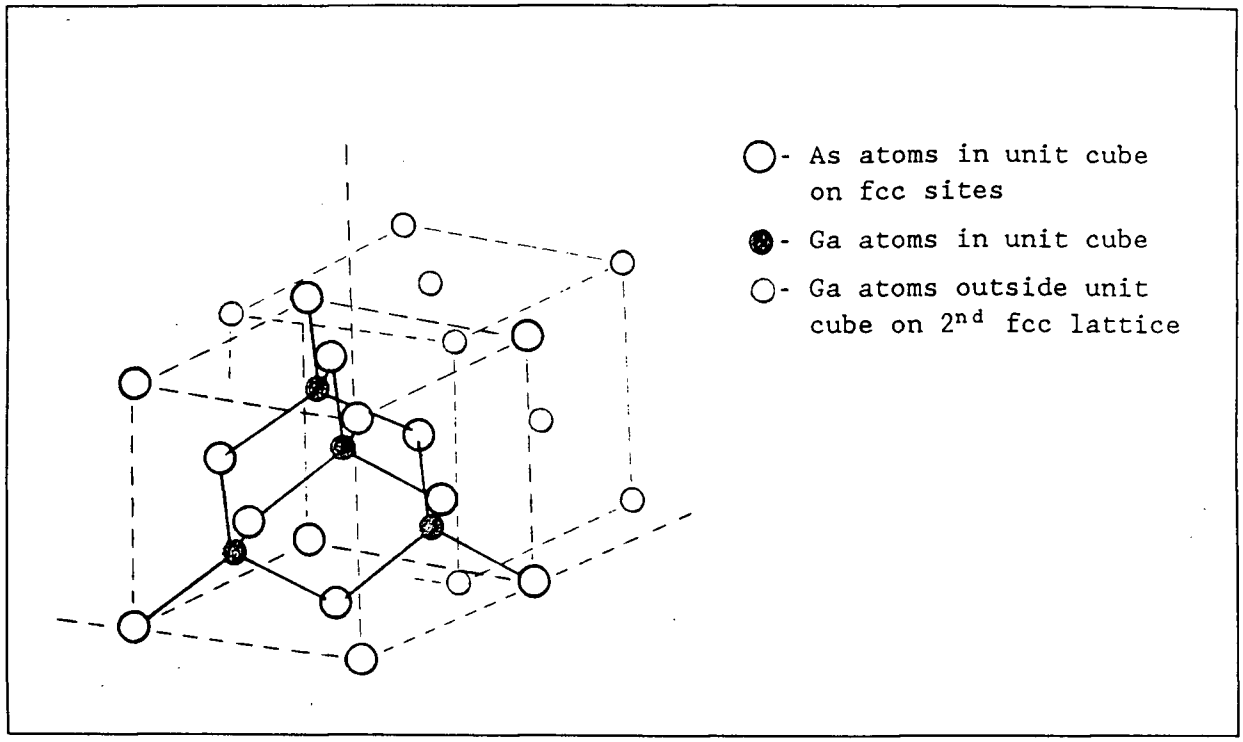

FIGURE 5. GaAs crystal structure (cubic zincblende) showing the two interpenetrating FCC lattices of Ga and As.

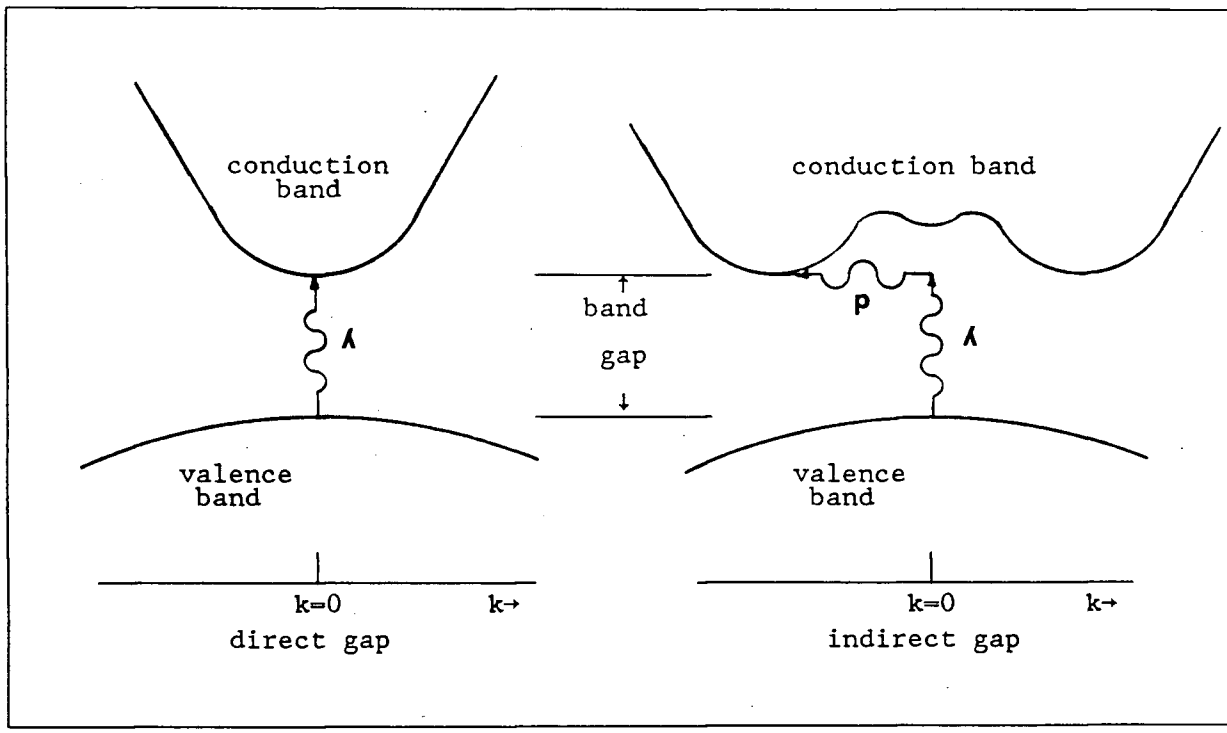

FIGURE 6. Schematic comparison of band structure of direct gap (left) and indirect gap (right) in momentum (k) space.

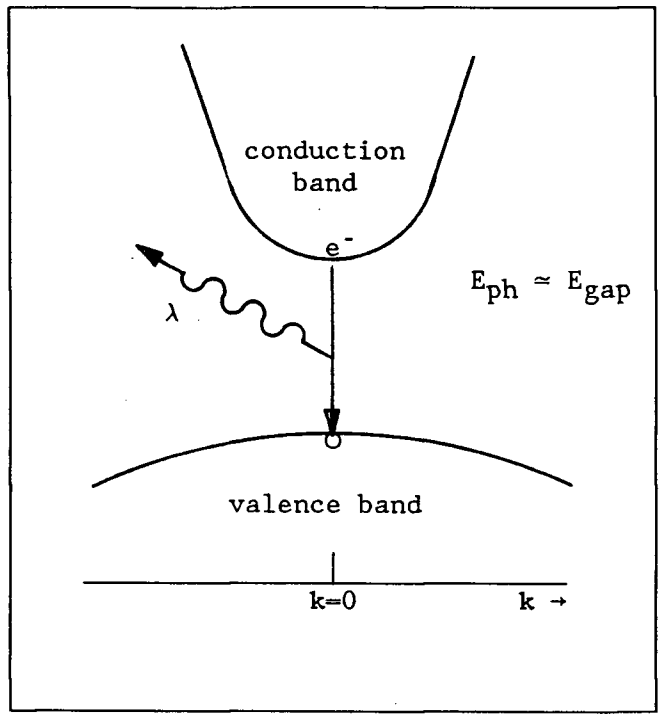

FIGURE 7. Schematic of simple, direct gap recombination.

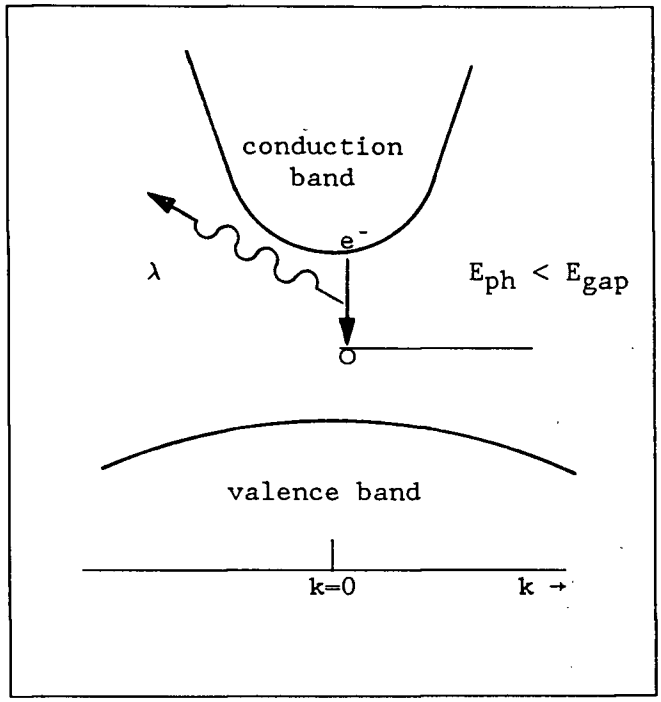

FIGURE 8. Schematic of recombination with an interband energy level.

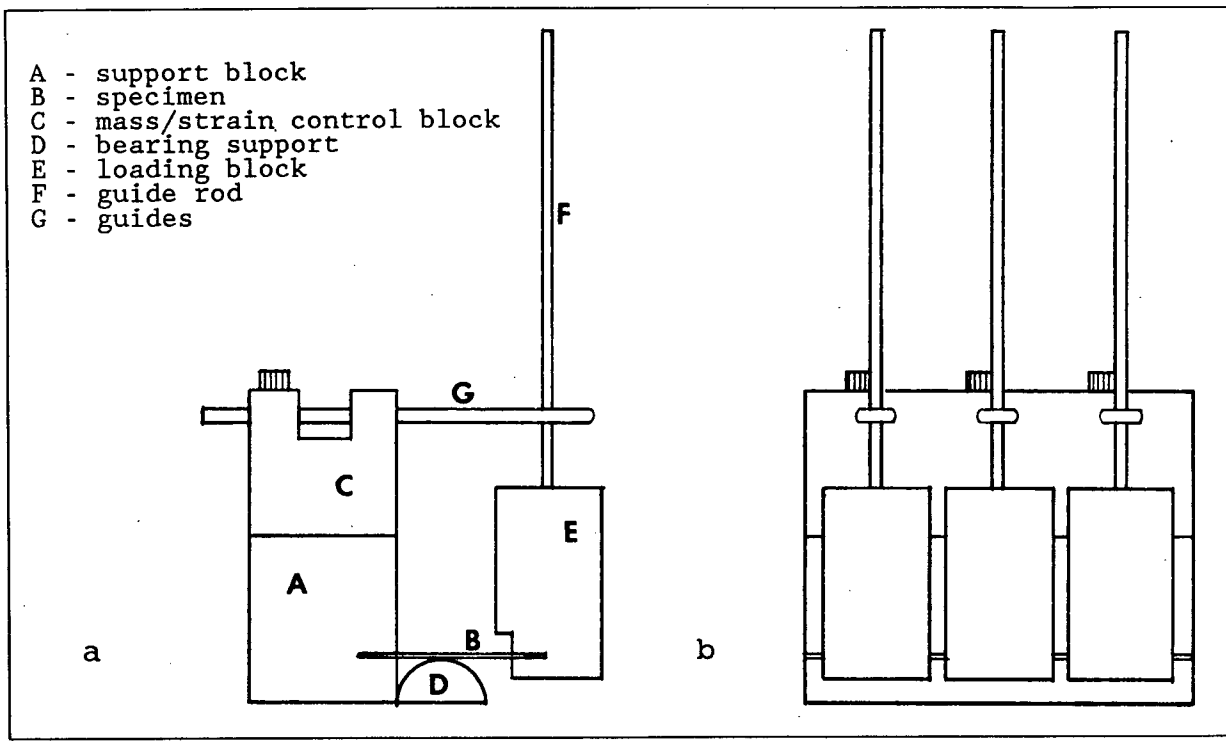

FIGURE 9. Static bending jig in profile (a) and showing arrangement (b).
scale 1:1

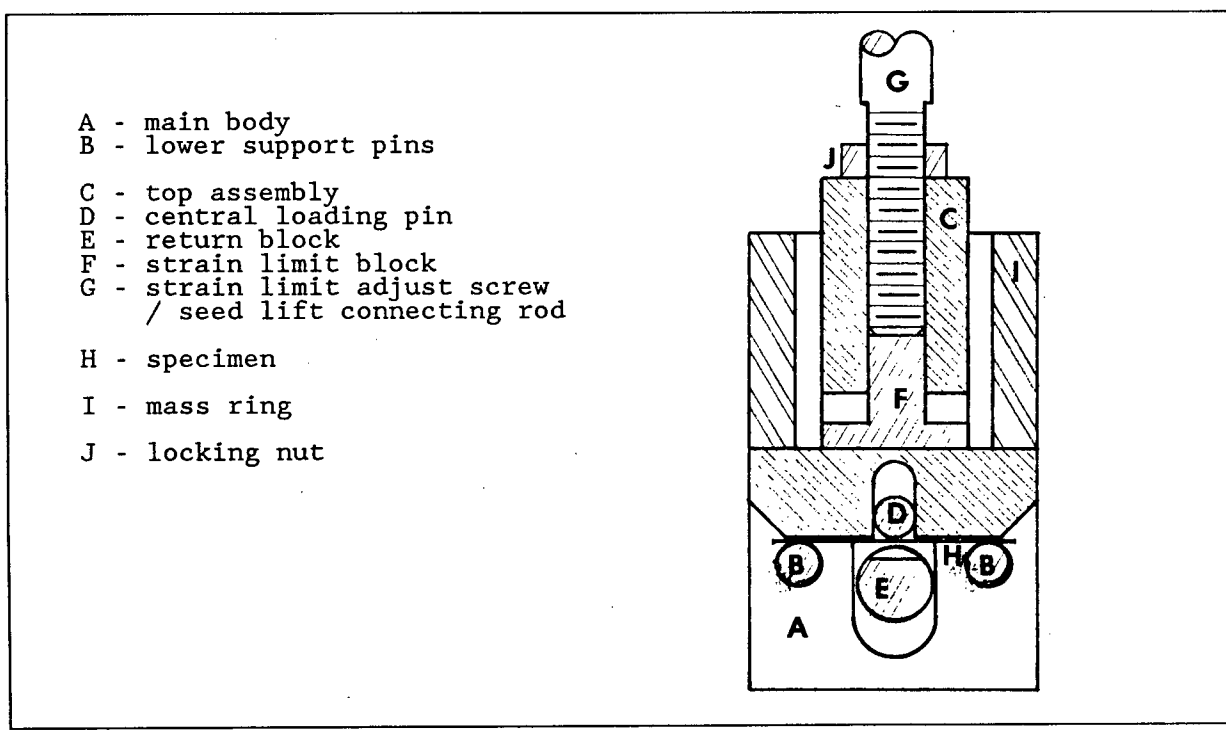

FIGURE 10. Dynamic bending jig shown in section. scale 1:1

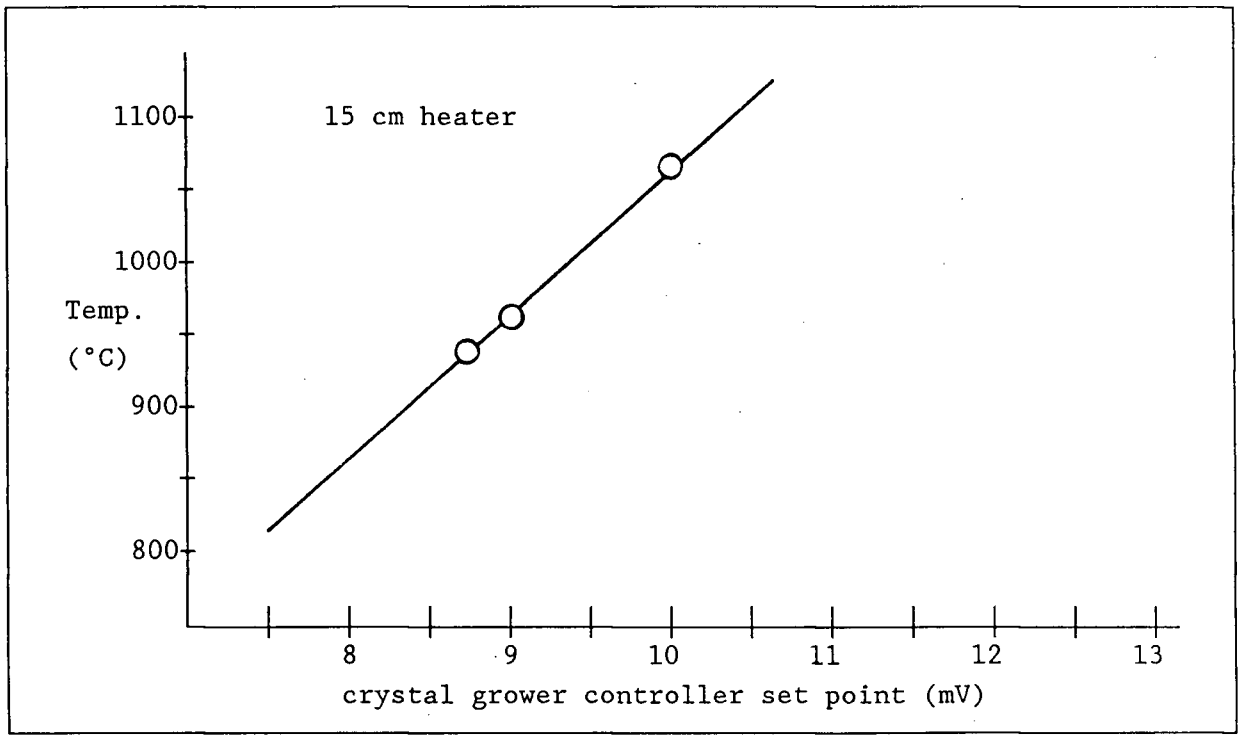

FIGURE 11. Calibration curve for crystal growers control thermocouple using the 15cm heater.

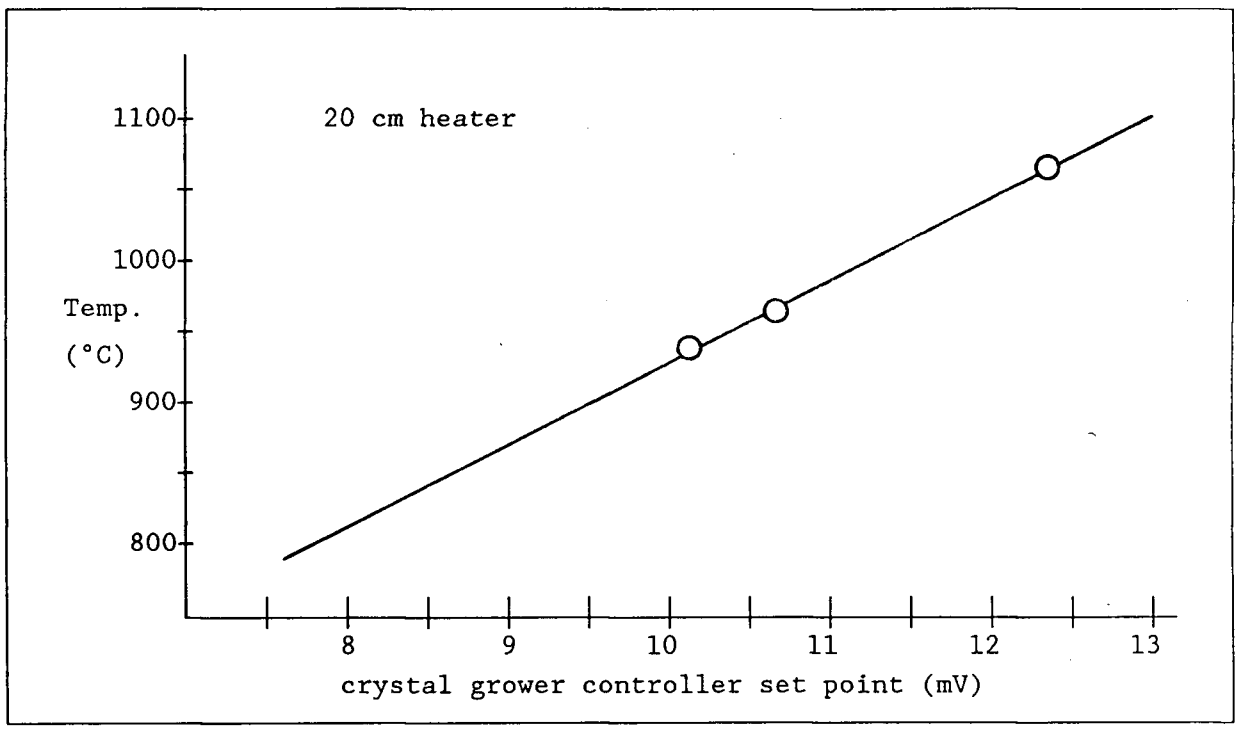

FIGURE 12. Calibration curve for crystal growers control thermocouple using the 20cm heater.

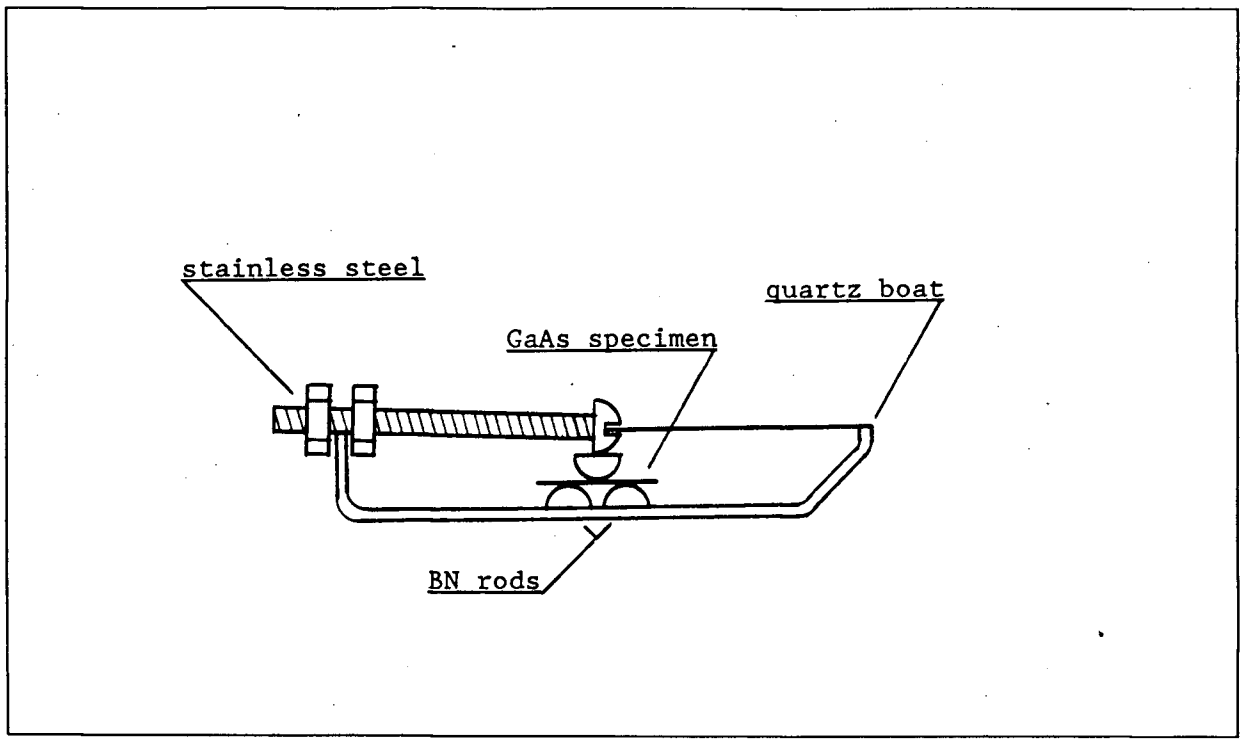

FIGURE 13. Experimental arrangement for testing B_2O_3 as an encapsulant for high temperature deformation of GaAs shown in section. scale 1:1.

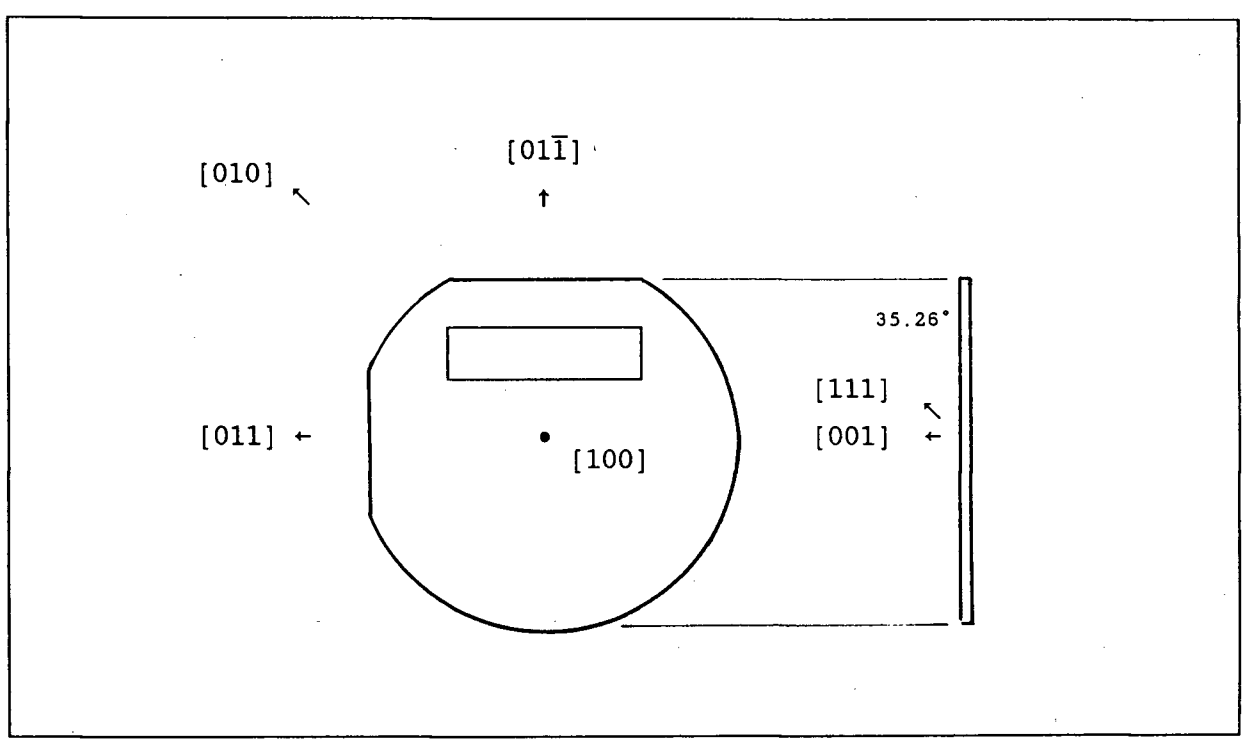

FIGURE 14. GaAs wafer orientation showing specimen alignment with wafer.

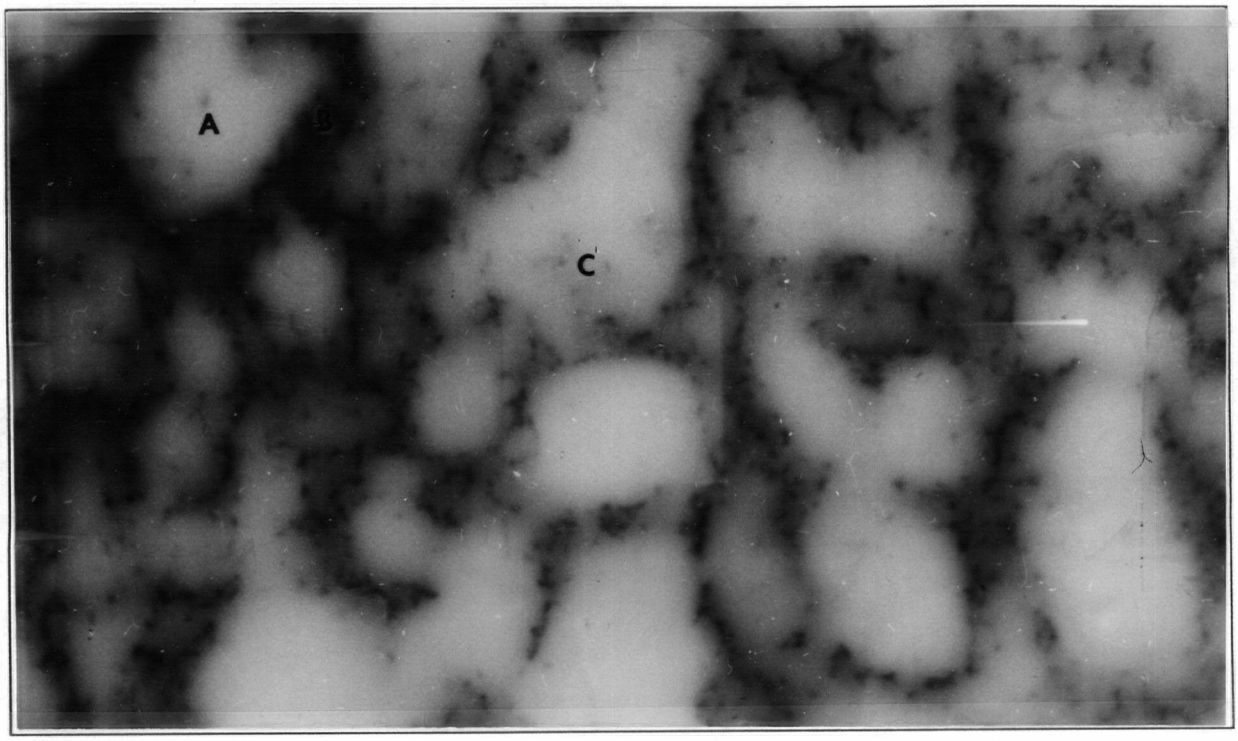

FIGURE 15. Inverted CL image of polished GaAs showing the networks of as-grown dislocation arrays. 32×

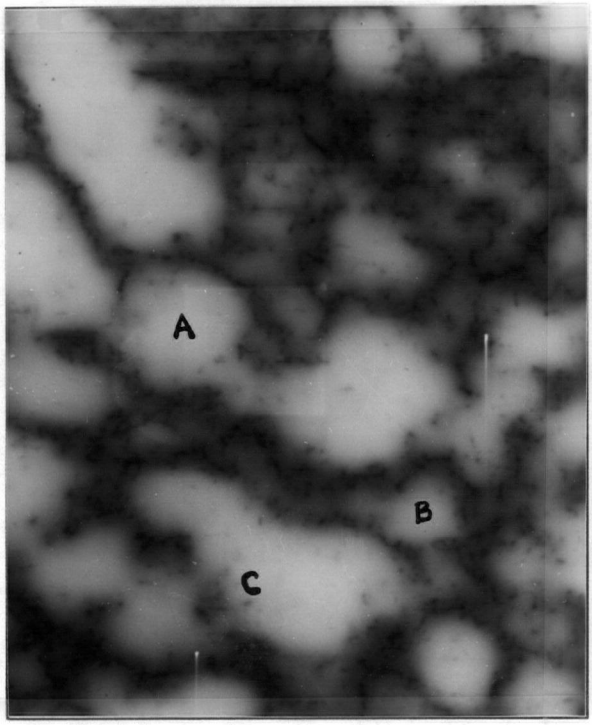

FIGURE 16. Inverted CL image of polished low grade GaAs showing dislocation arrays and spots. 32×

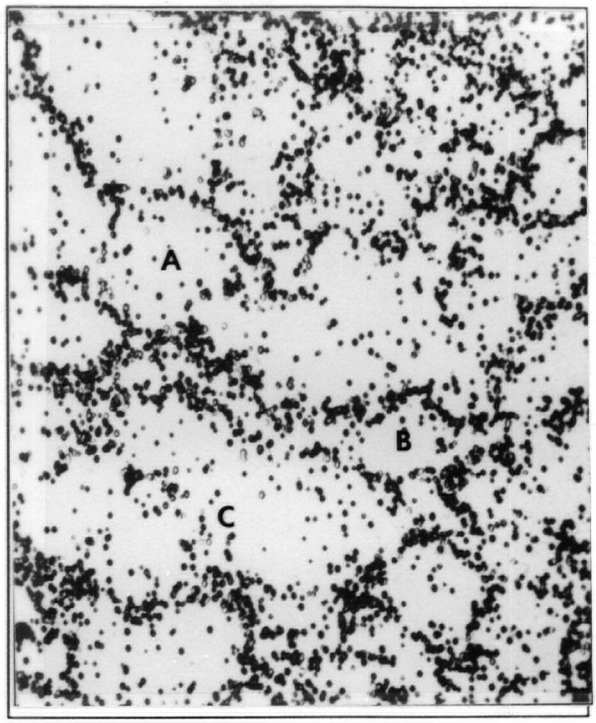

FIGURE 17. Optical image of same GaAs surface as in Figure 16 after a chemical etch in molten KOH. 32×

FIGURE 18. CL image of etched (KOH) low dislocation density GaAs. 32×

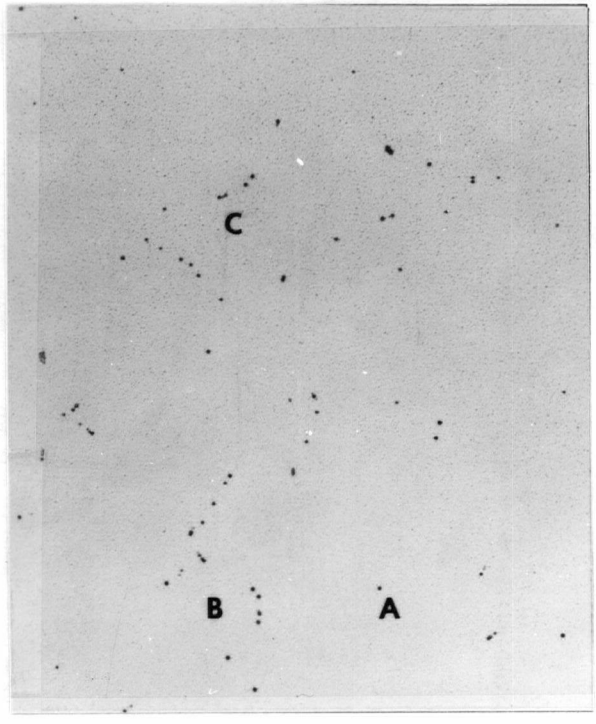

FIGURE 19. Optical image of same area of GaAs as in Figure 18, showing etch pits. 32×

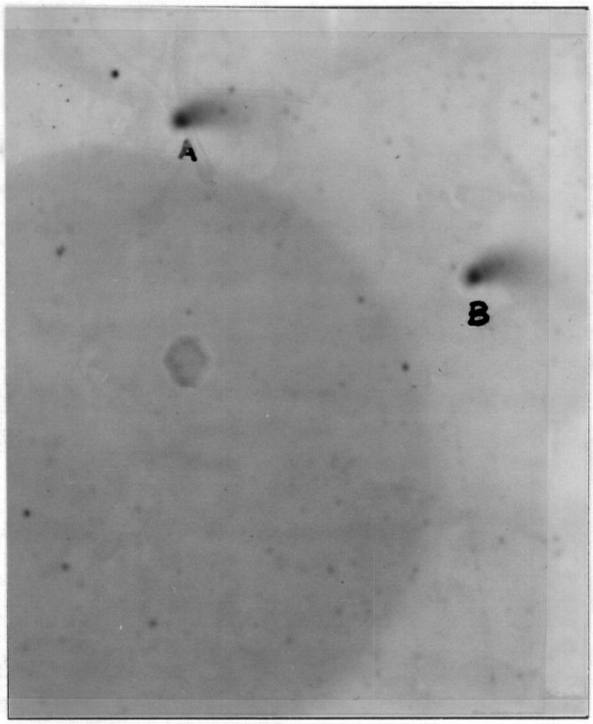

FIGURE 20. CL image of sample of Si doped GaAs, KOH etched. 128×

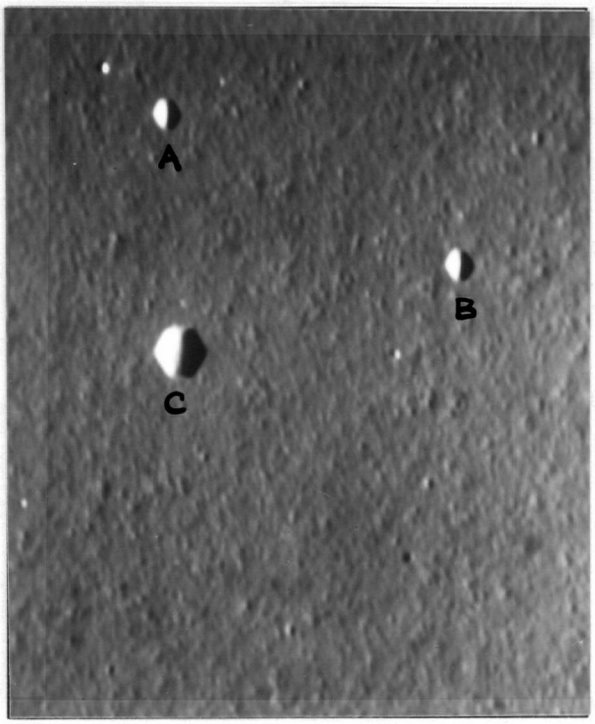

FIGURE 21. SE image of same area of Si doped GaAs as in Figure 20, showing KOH etch pits. 128×

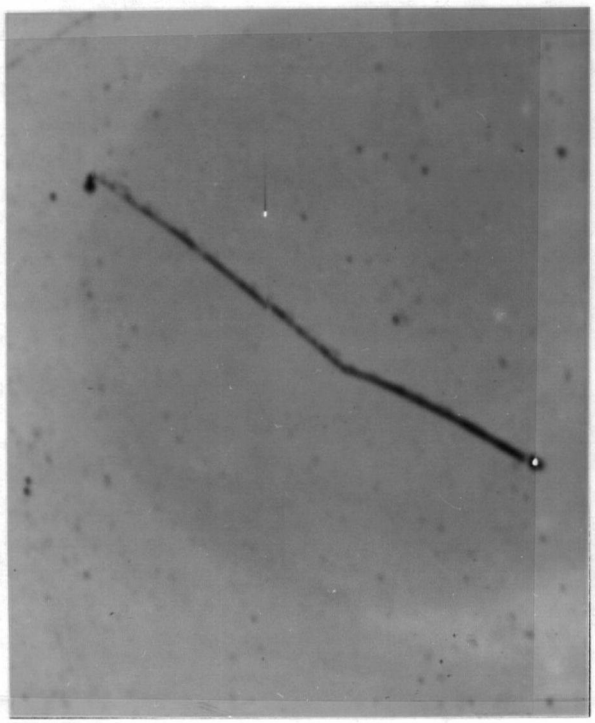

FIGURE 22. CL image of a dislocation parallel to the surface of Si doped GaAs. 128×

FIGURE 23. SE image of same area of etched GaAs as in Figure 22 showing absence of etch pits. 128×

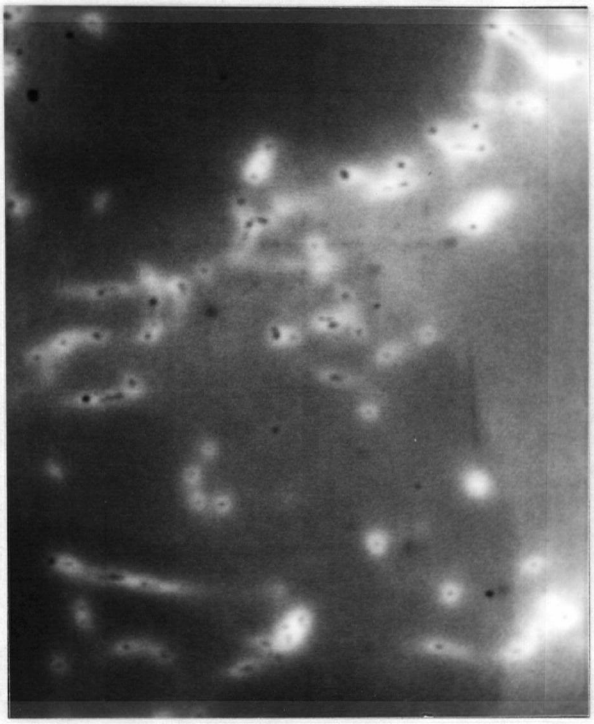

FIGURE 24. CL image of electronics grade GaAs showing "dots" and "halos" effects around dislocations. 128×

FIGURE 25. CL image of GaAs after heating to 1000°C. 52×

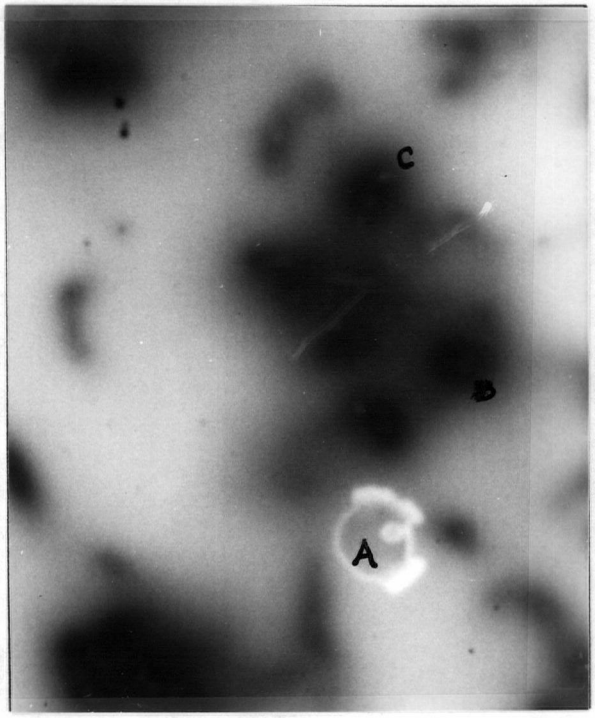

FIGURE 26. Enlarged CL image of GaAs from region of Figure 25. 128×

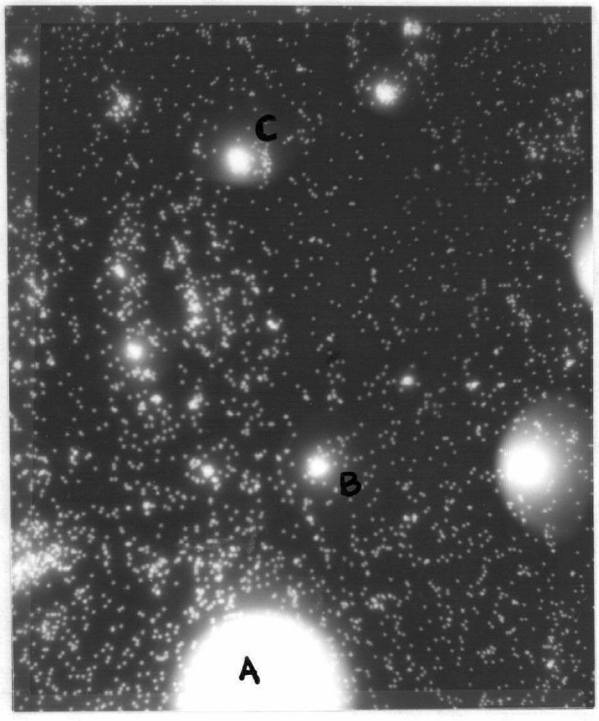

FIGURE 27. SIMS map of GaAs from the same region as Figure 26, showing distribution of carbon. 140×

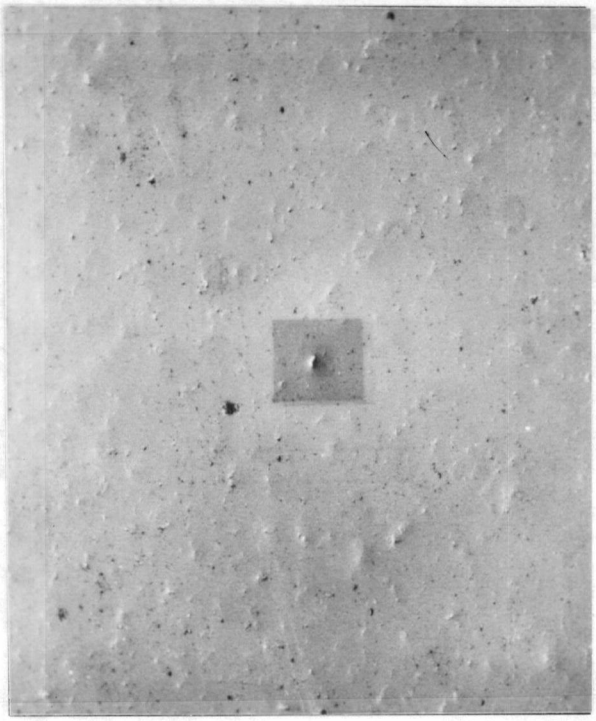

FIGURE 28. SE image of 750Å thick Si_3N_4 cap on GaAs. 200×

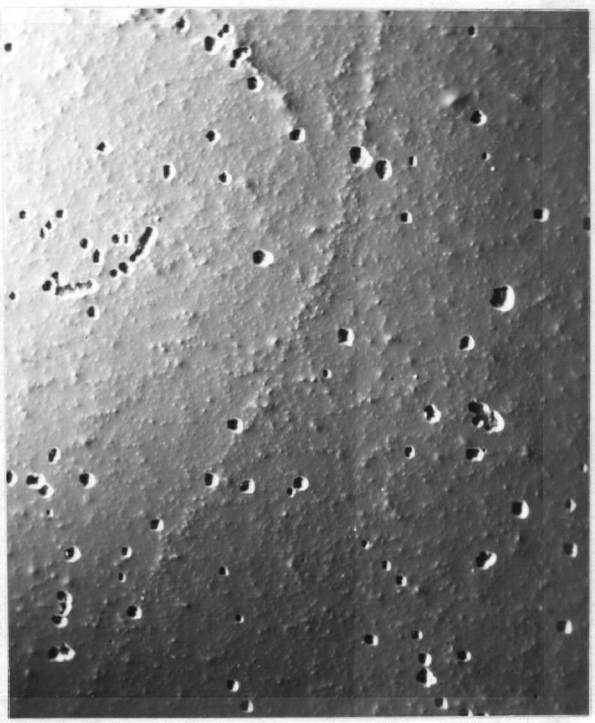

FIGURE 29. SE image of pits in Si_3N_4 cap on GaAs that formed after heating to 950°C. 32×

FIGURE 30. CL image of capped GaAs after heating to 950°C, from the same area as Figure 29. 32×

FIGURE 31. Inverted CL image of capped GaAs specimen T4. 32×

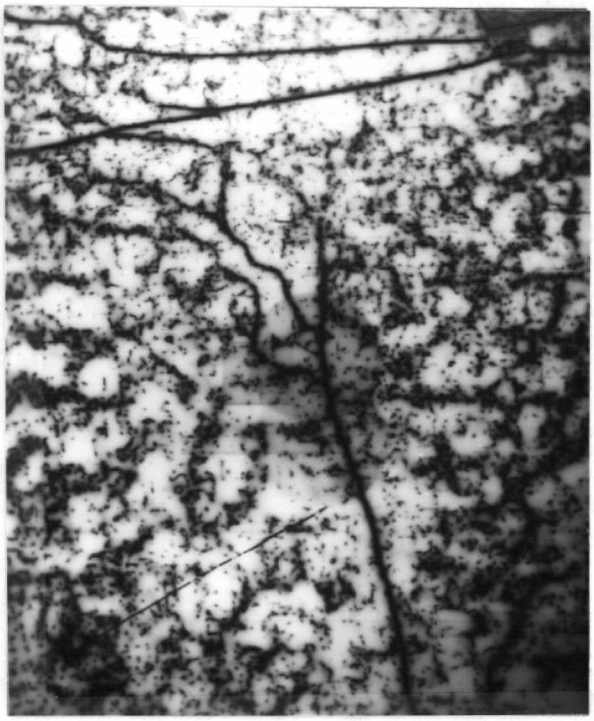

FIGURE 32. CL image of GaAs specimen T4 after 360s anneal @ 955°C. Si_3N_4 cap removed and surface polished. Same area as Figure 31. 32×

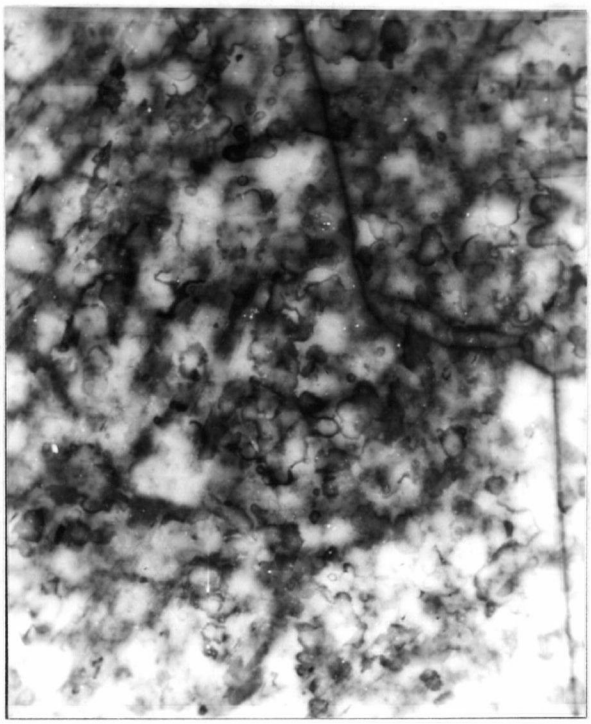

FIGURE 33. Inverted CL image of capped GaAs T4, adjacent region to Figure 31. 32×

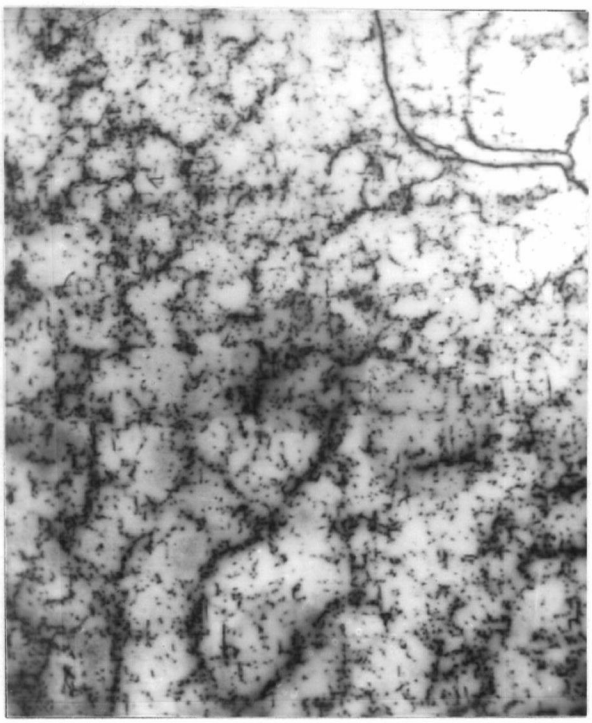

FIGURE 34. CL image of annealed GaAs T4 from area adjacent to Figure 32, same area as Figure 33. 32×

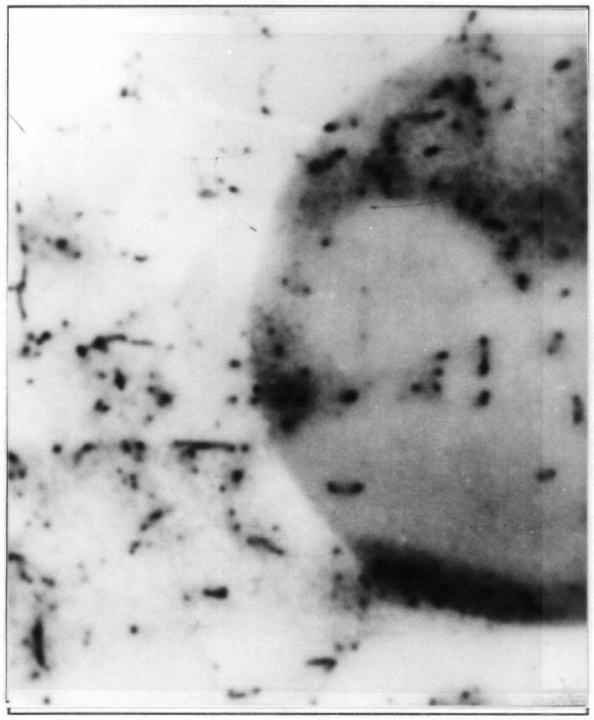

FIGURE 35. CL image of GaAs T2 after heating to 955°C and bending. Area 12.5mm from bend axis. 128×

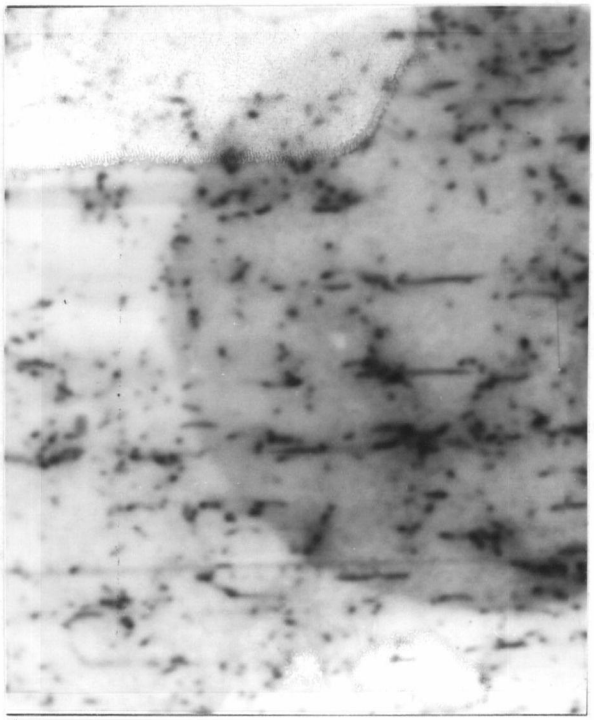

FIGURE 36. CL image of GaAs T2 after heating to 955°C and bending. Area 7.5mm from bend axis. 128×

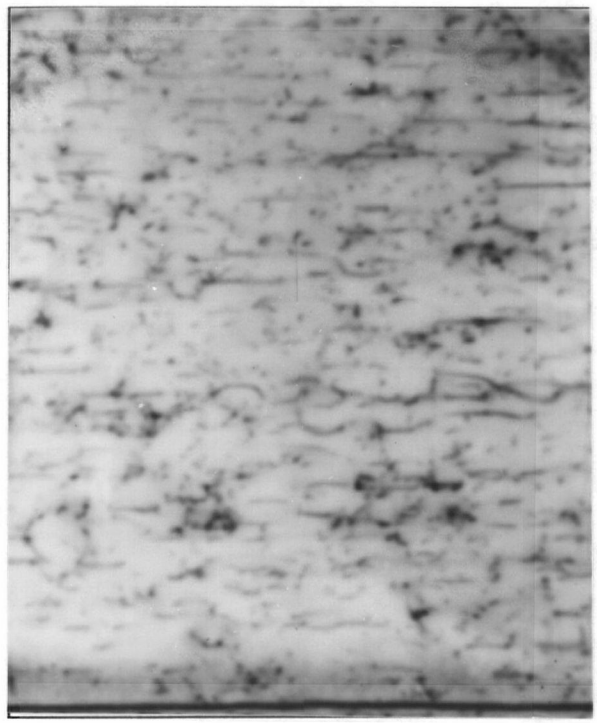

FIGURE 37. CL image of GaAs T2 After heating to 955°C and bending. Area 3mm from bend axis. 128×

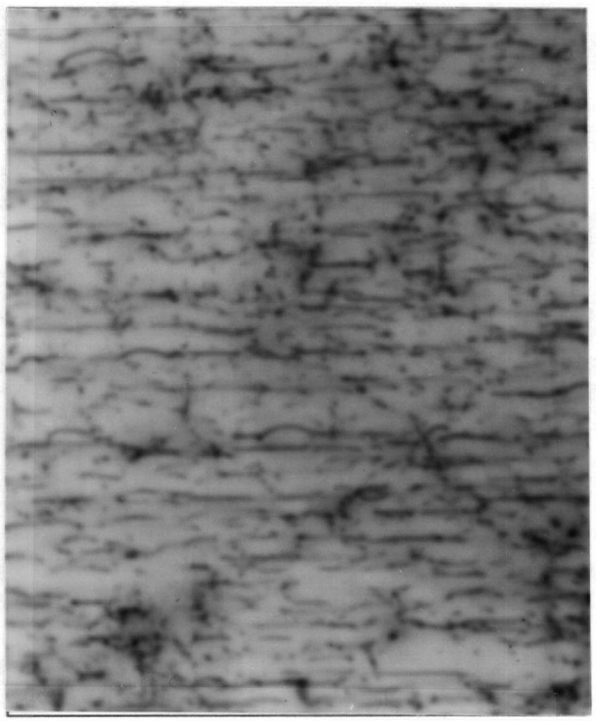

FIGURE 38. CL image of GaAs T2 after heating to 955°C and bending. Area 1.5mm from bend axis. 128×

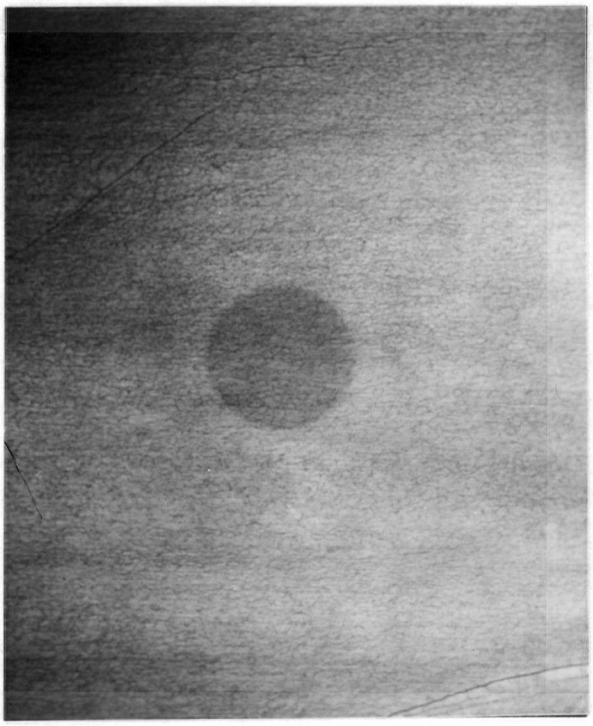

FIGURE 39. CL image of GaAs T5 after heating to 955°C and bending. Area near bend axis. 32×

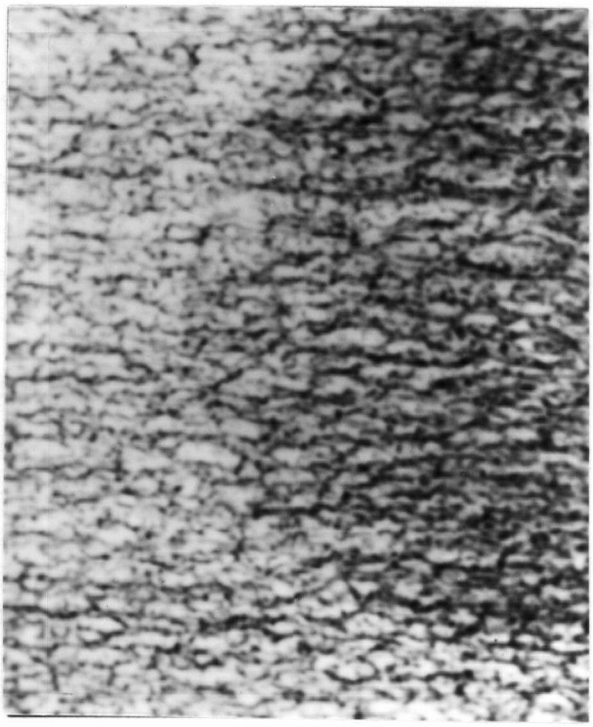

FIGURE 40. CL image of GaAs T5 showing new dislocation arrays in area of Figure 39. 128×

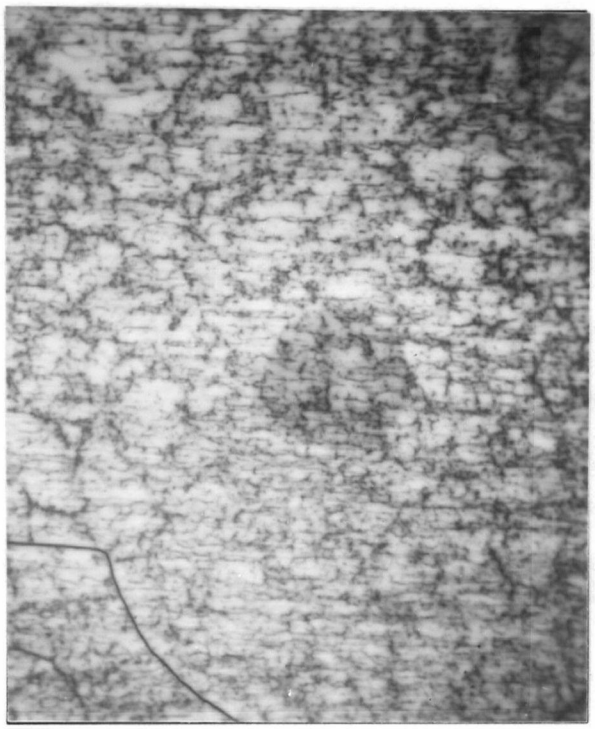

FIGURE 41. CL image of GaAs T5 after heating and bending. Area away from bend axis. 32×

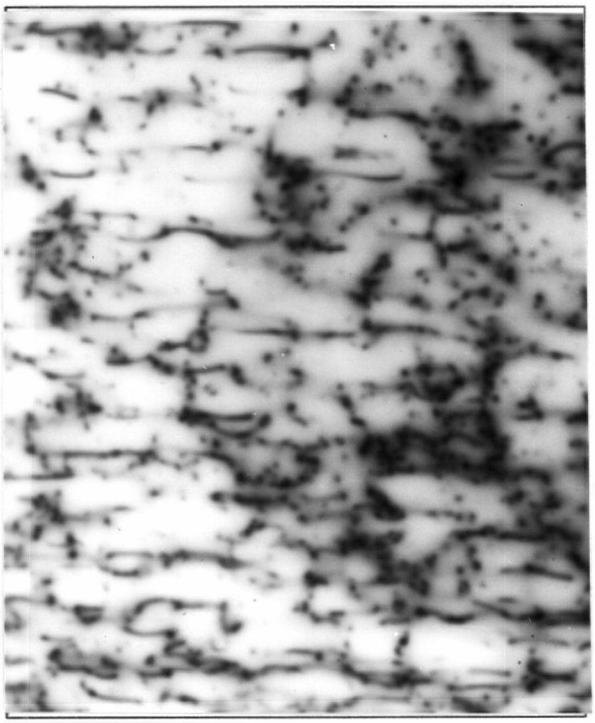

FIGURE 42. CL image of GaAs T5 showing new arrays from area in Figure 41. 128×

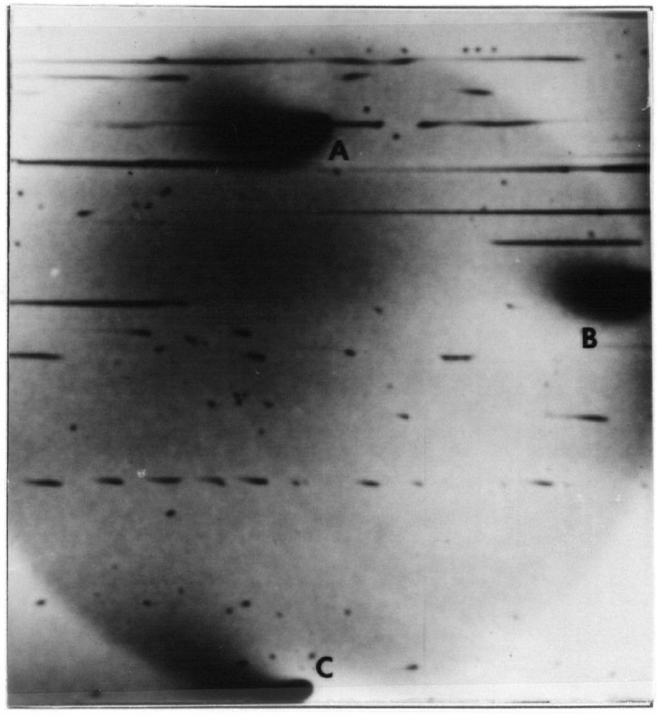

FIGURE 43. CL image of Si doped GaAs Si1 after heating to 955°C and bending, showing old and new dislocations in low strain region. 128×

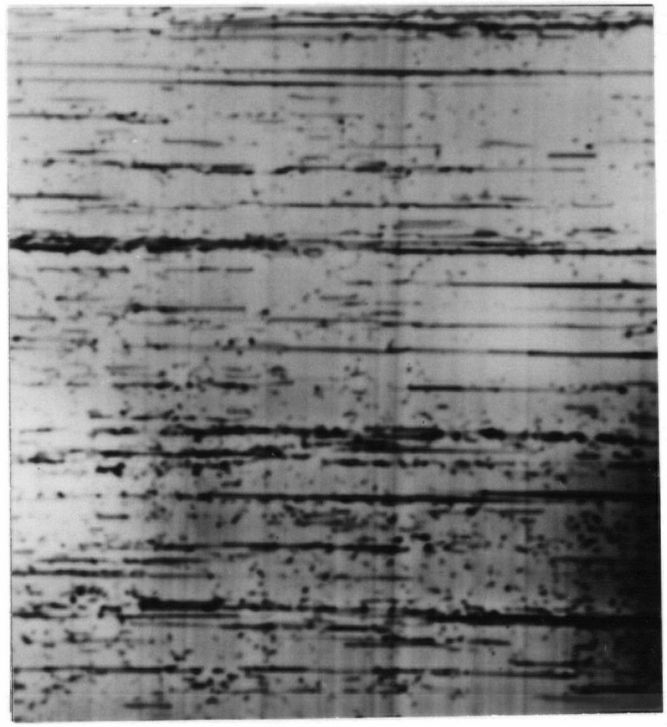

FIGURE 44. CL image of Si doped GaAs Si1 after heating and bending showing new arrays in the high strain region. 128×

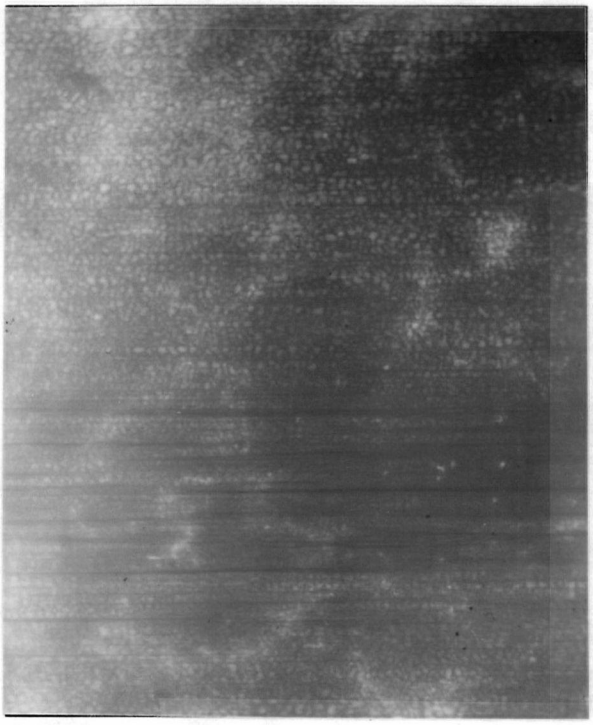

FIGURE 45. CL image of GaAs S1 after heating to 1000°C & cyclic loading. Area near bend axis. 32×

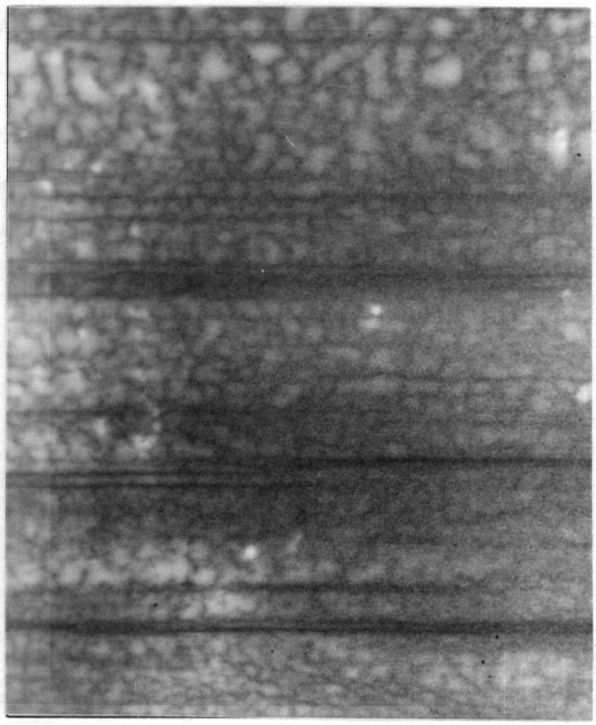

FIGURE 46. CL image of dislocation arrays in area of Figure 45. 128×

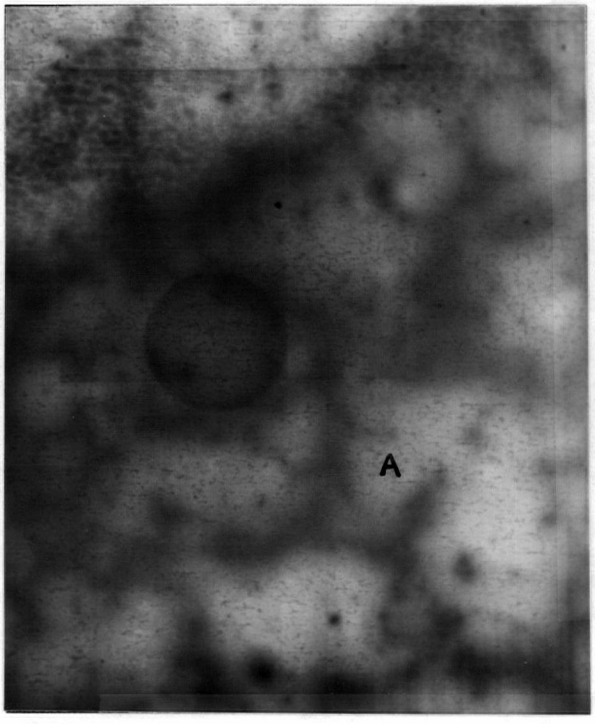

FIGURE 47. CL image of S1 after heating & cycling from the area away from the bend axis. 32×

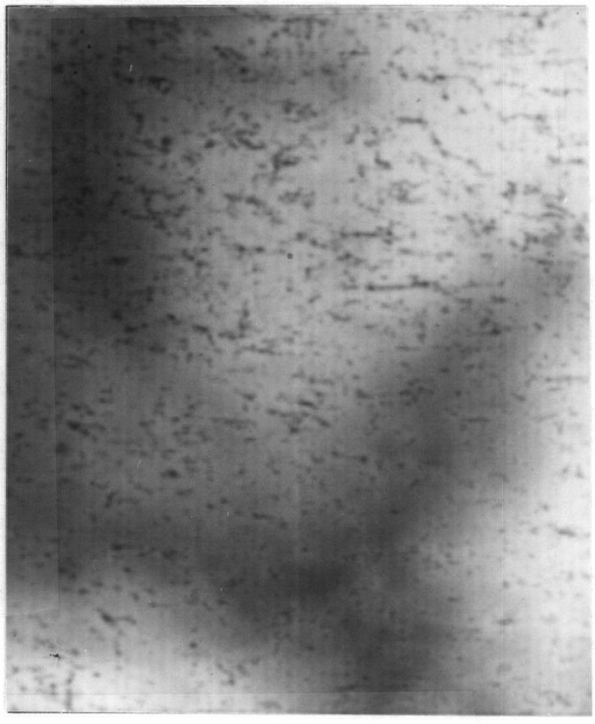

FIGURE 48. CL image of dislocation arrays in area of Figure 47. 128×

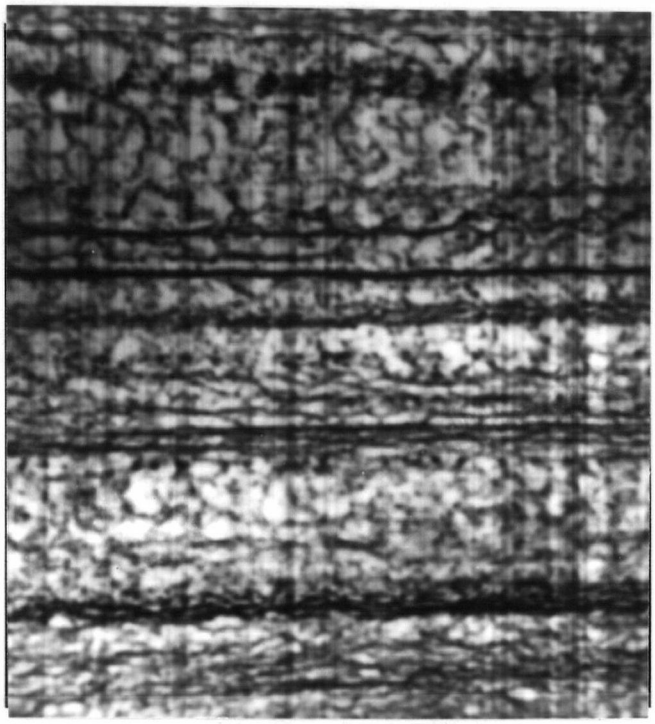

FIGURE 49. CL image of GaAs S2 showing dislocation arrays after cycling at 1050°C. Near the bend axis. 128×

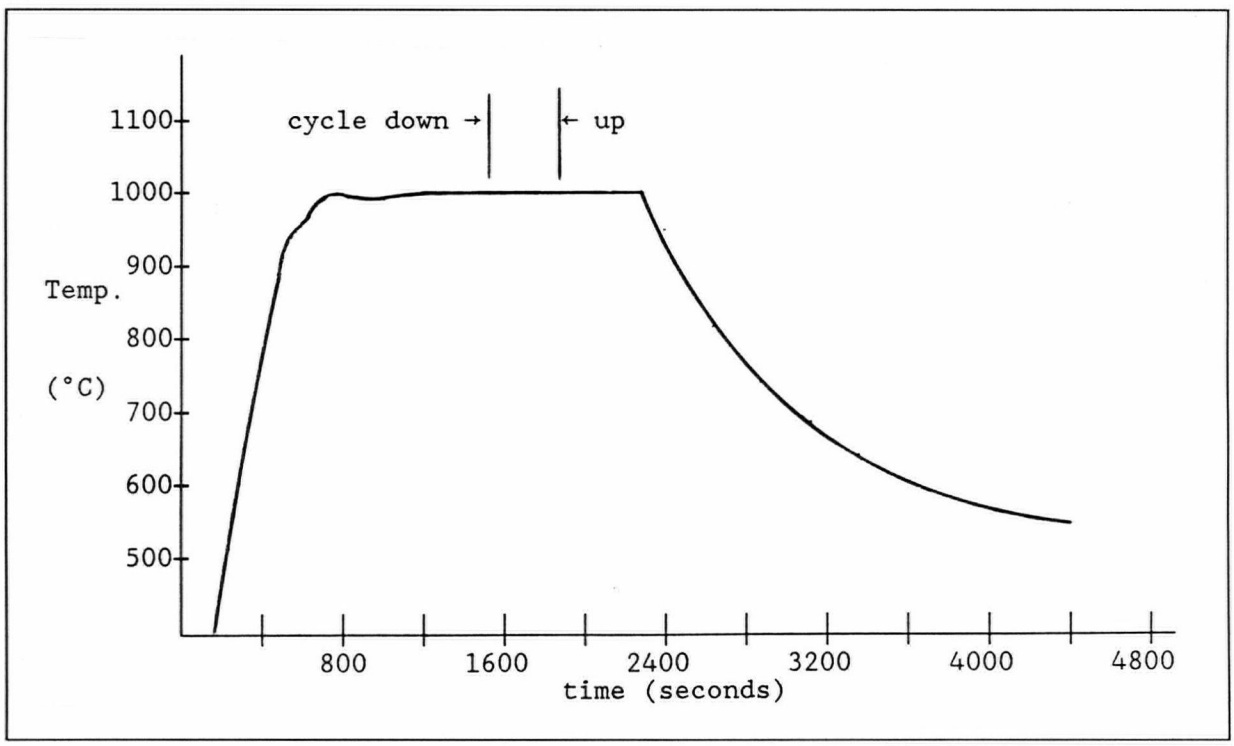

FIGURE 50. Thermal history of GaAs specimen S3 during high temperature bend.

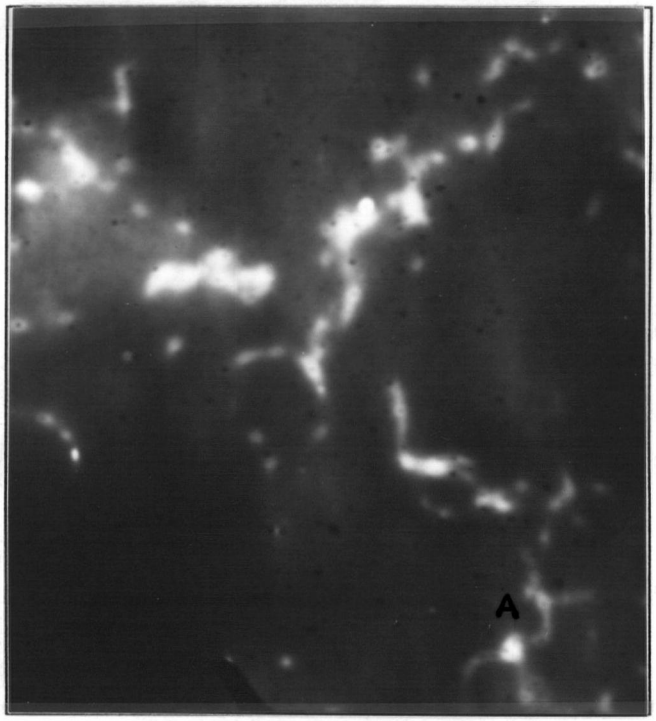

FIGURE 51. CL image of GaAs sample S3 capped with 800Å of Si_3N_4 taken 6mm from the centre of the specimen. 128×

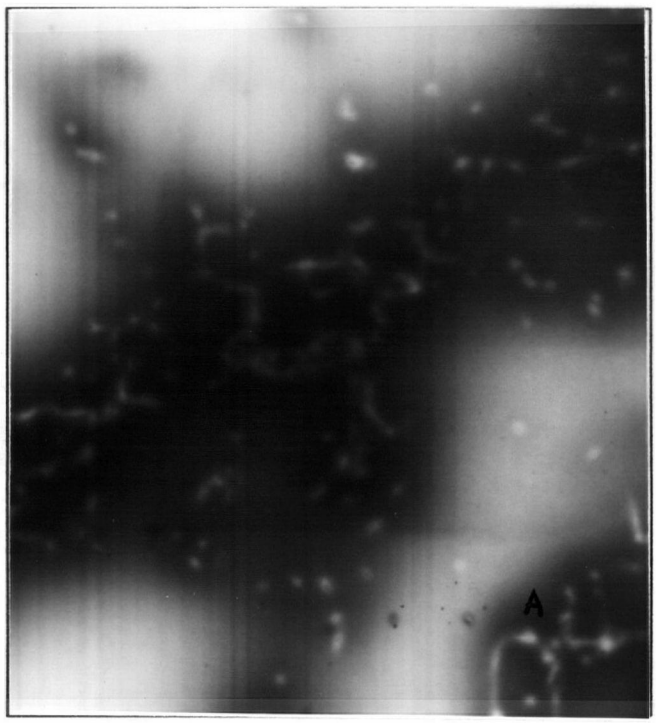

FIGURE 52. CL image of same area of S3 as Figure 51 after bending @ 1000°C. Low strain region 6mm from bend axis. 128×

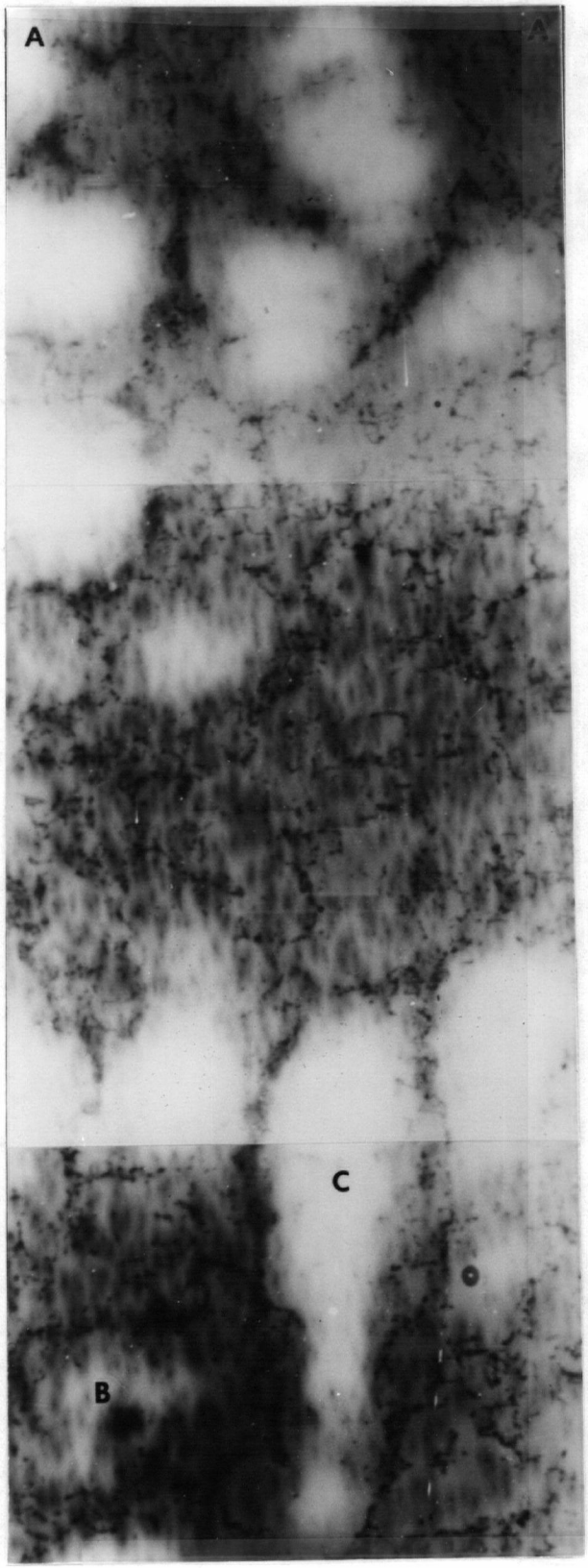

FIGURE 53. Inverted CL image map of middle 12mm of GaAs specimen S3 capped with 800Å of Si_3N_4. 32×

FIGURE 54. CL image map of GaAs S3 after 1 bending cycle @ 1000°C. Same region as Figure 53. 32×

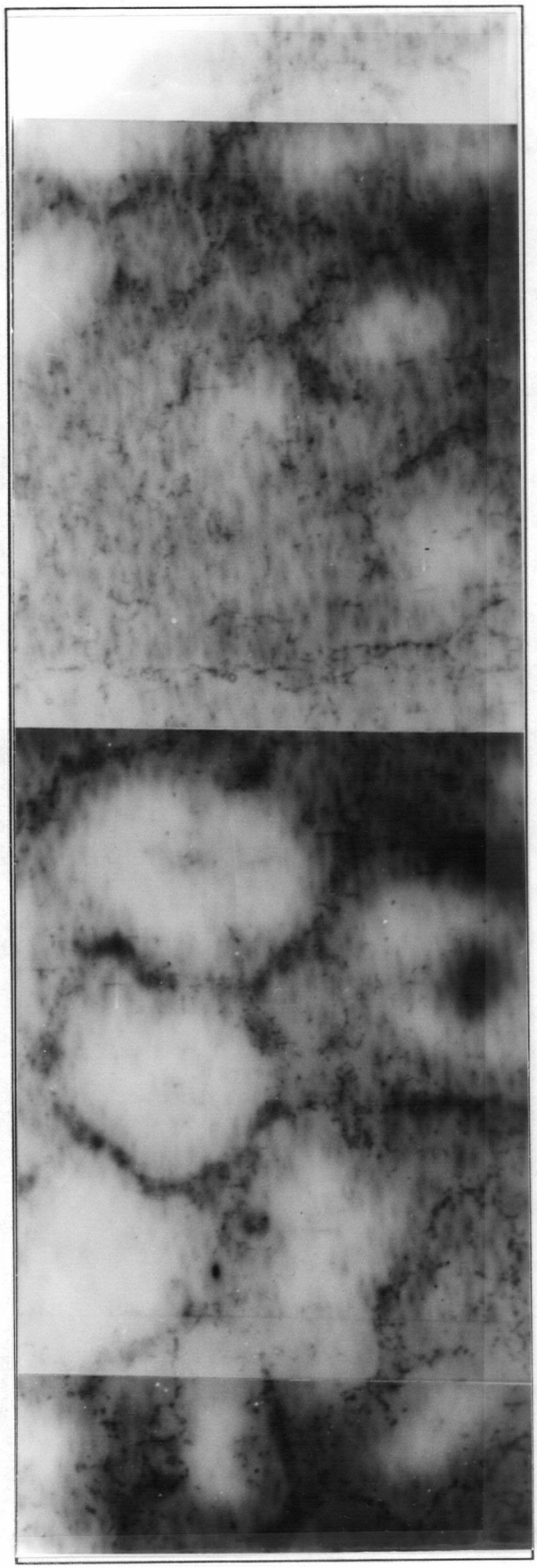

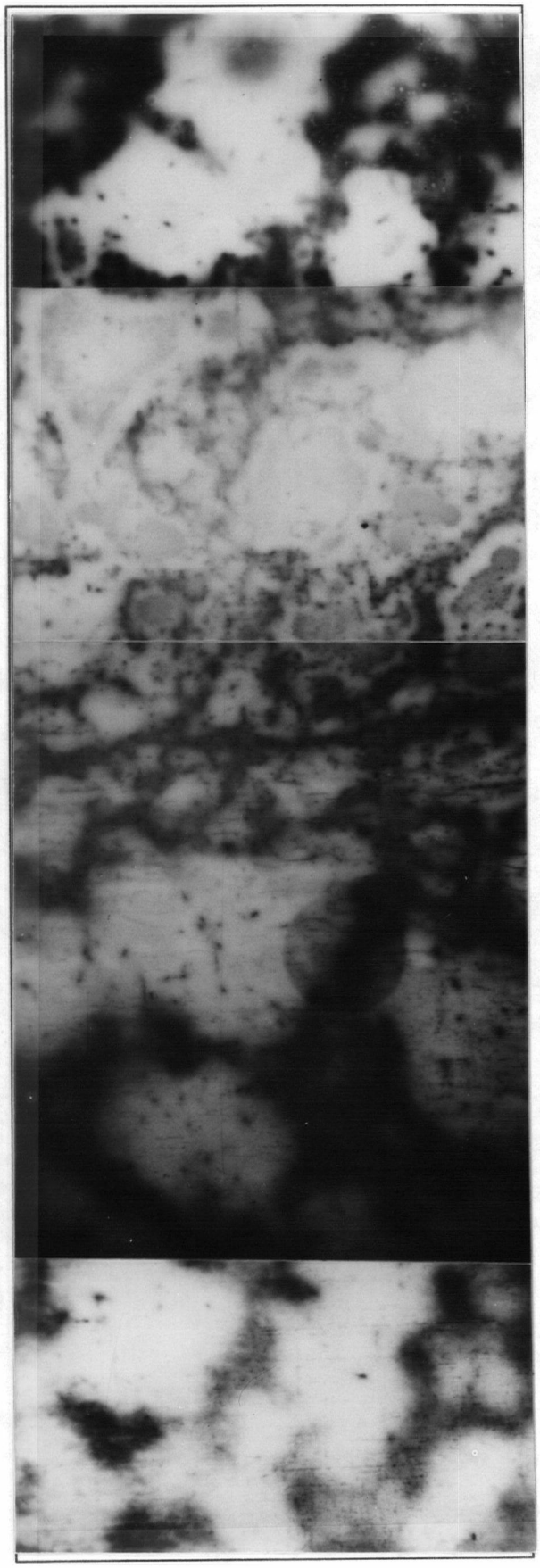

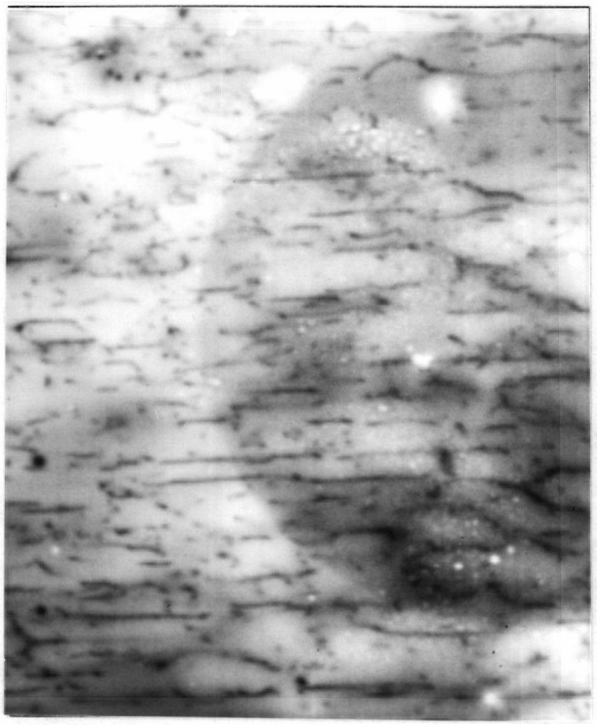

FIGURE 55. CL image of GaAs S4 after cycling at 1000°C. Highest strain region, at the bend axis. 128×

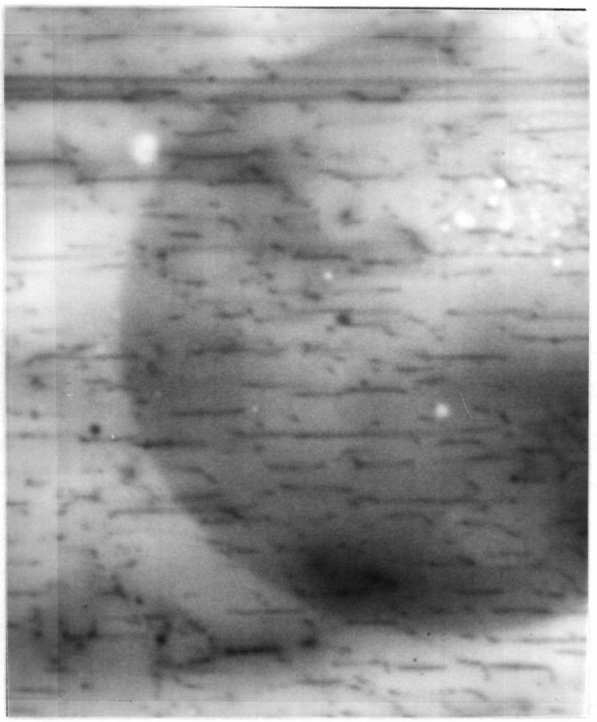

FIGURE 56. CL image of GaAs S4 adjacent to region in Figure 55, near the bend axis. 128×

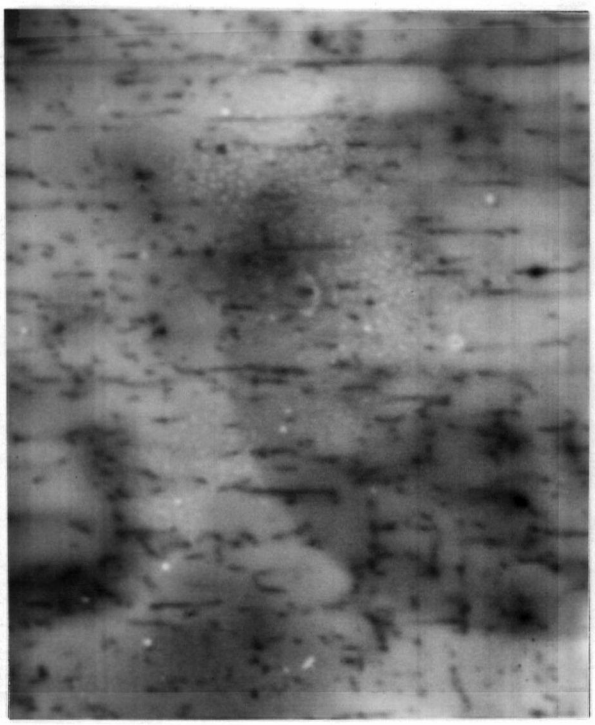

FIGURE 57. CL image of GaAs S4 region away from the bend axis, in the bright zone. 128×

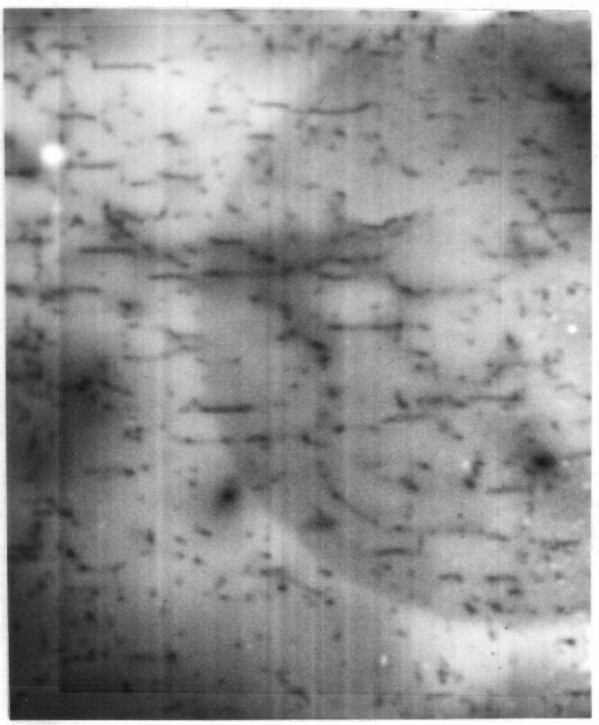

FIGURE 58. CL image of GaAs S4 region further away from the bend axis, in the bright zone. 128×

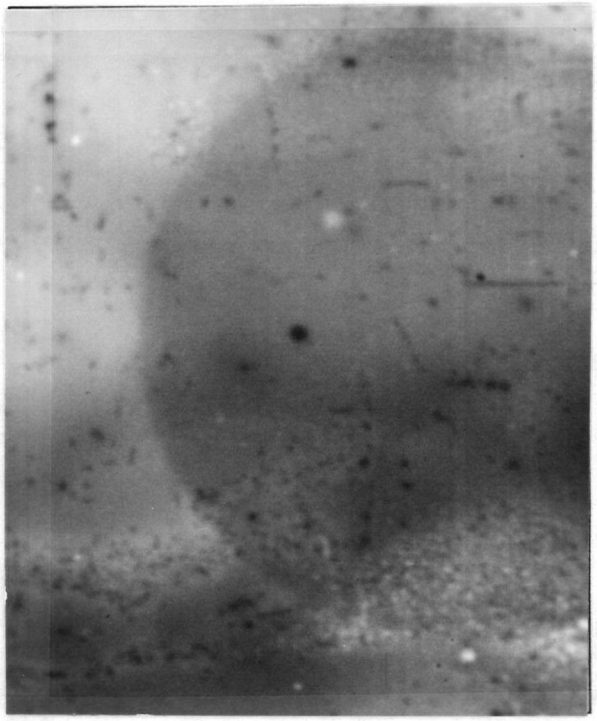

FIGURE 59. CL image of GaAs S4 after cycling at 1000°C. Low strain area in the bright zone near transition. 128×

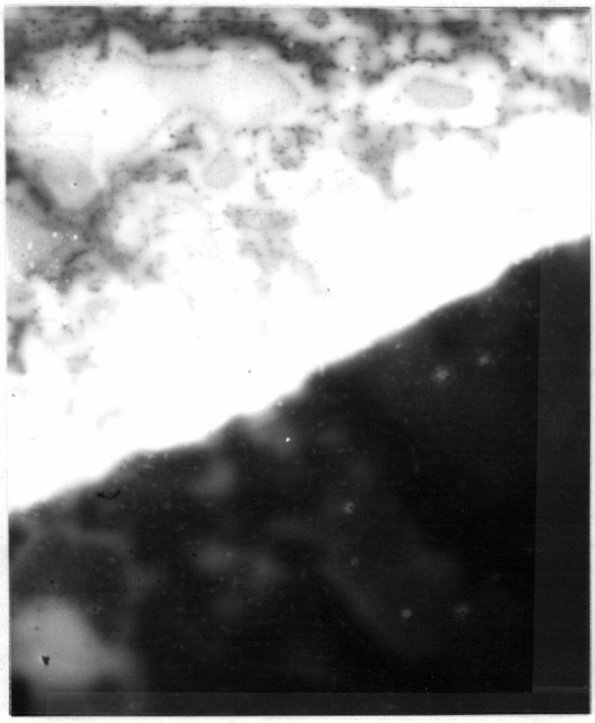

FIGURE 60. CL image of GaAs S4 at the transition from the bright zone to the dark zone. 32×

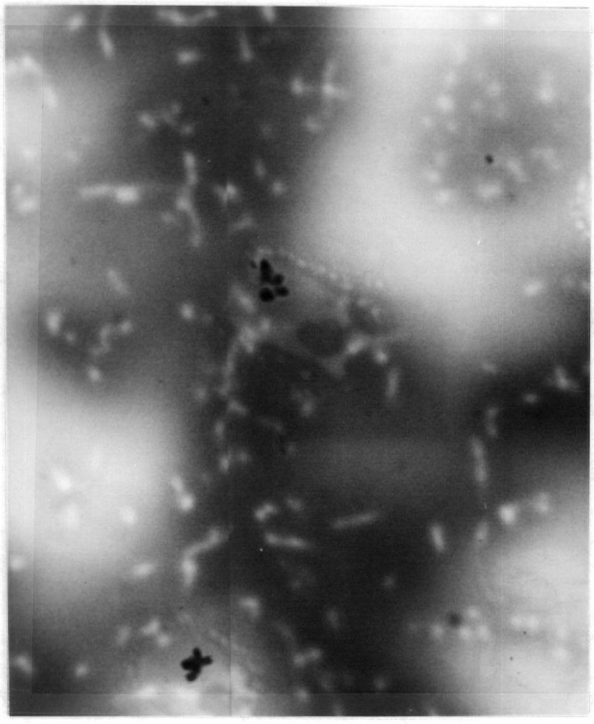

FIGURE 61. CL image of GaAs S4 showing dislocation distribution in the dark zone. 128×

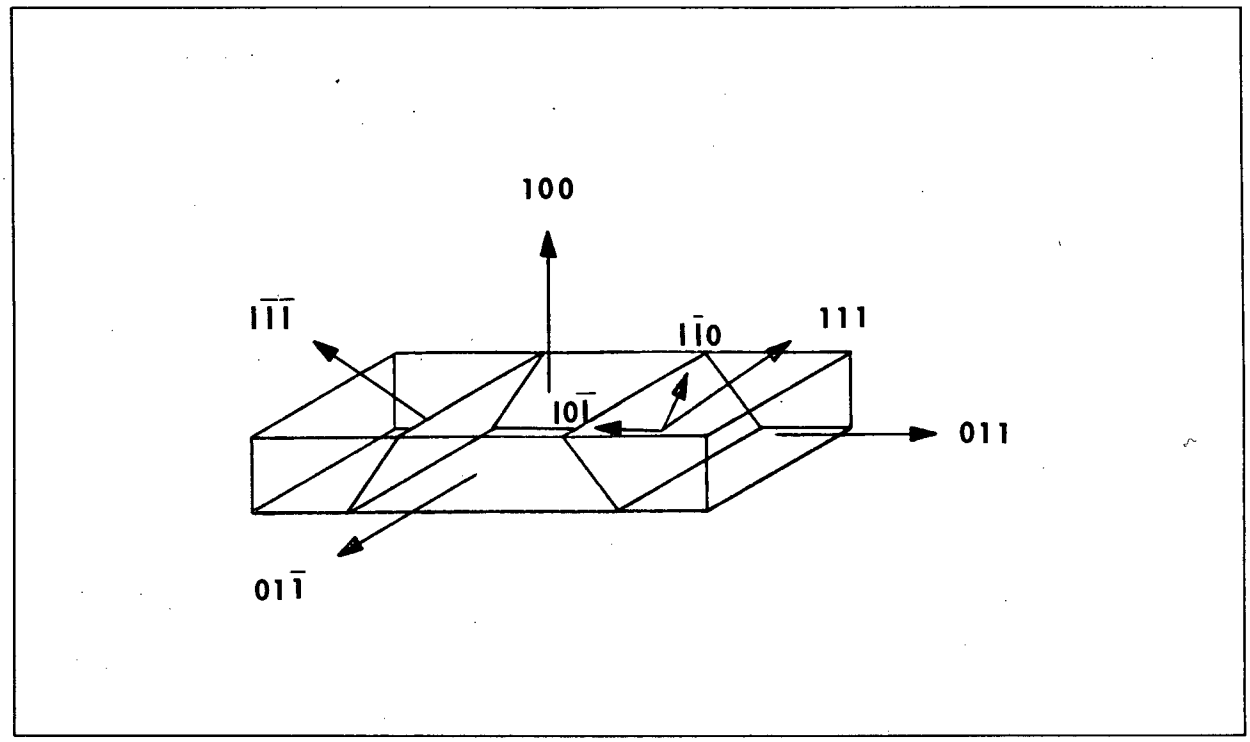

FIGURE 62. Slip planes and slip directions in bend specimens.

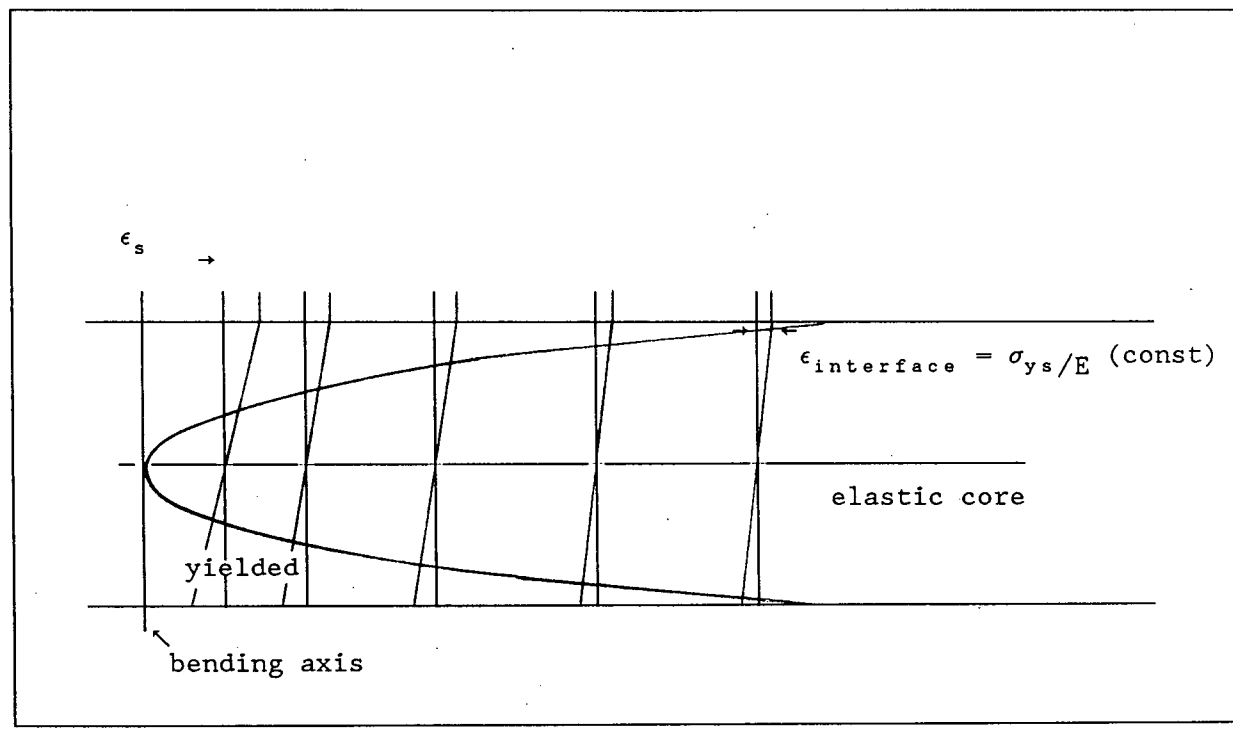

FIGURE 63. Construction showing surface strain (ϵ_s) due to a varying yield depth (YD) for a calculated YD profile in a 3-point bend specimen.

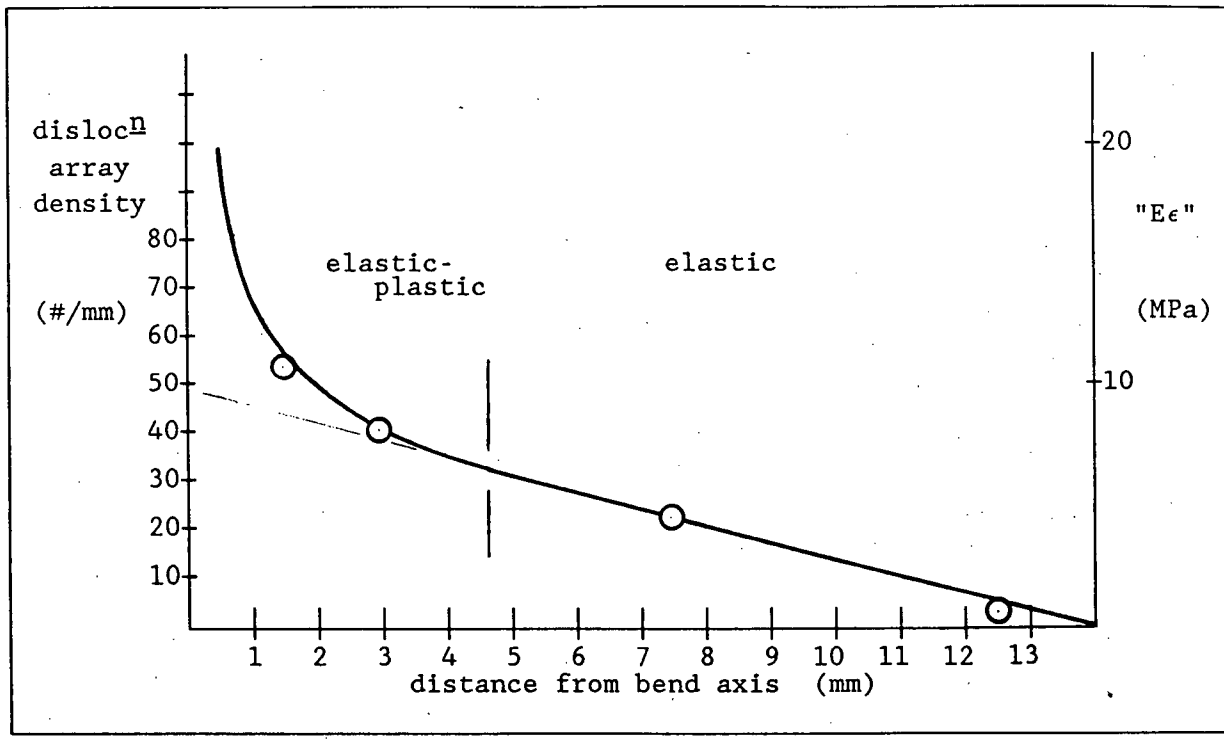

FIGURE 64. Dislocation line density versus distance from bend axis for GaAs specimen T2 plus parametric curve of "Eε" scaled to data.

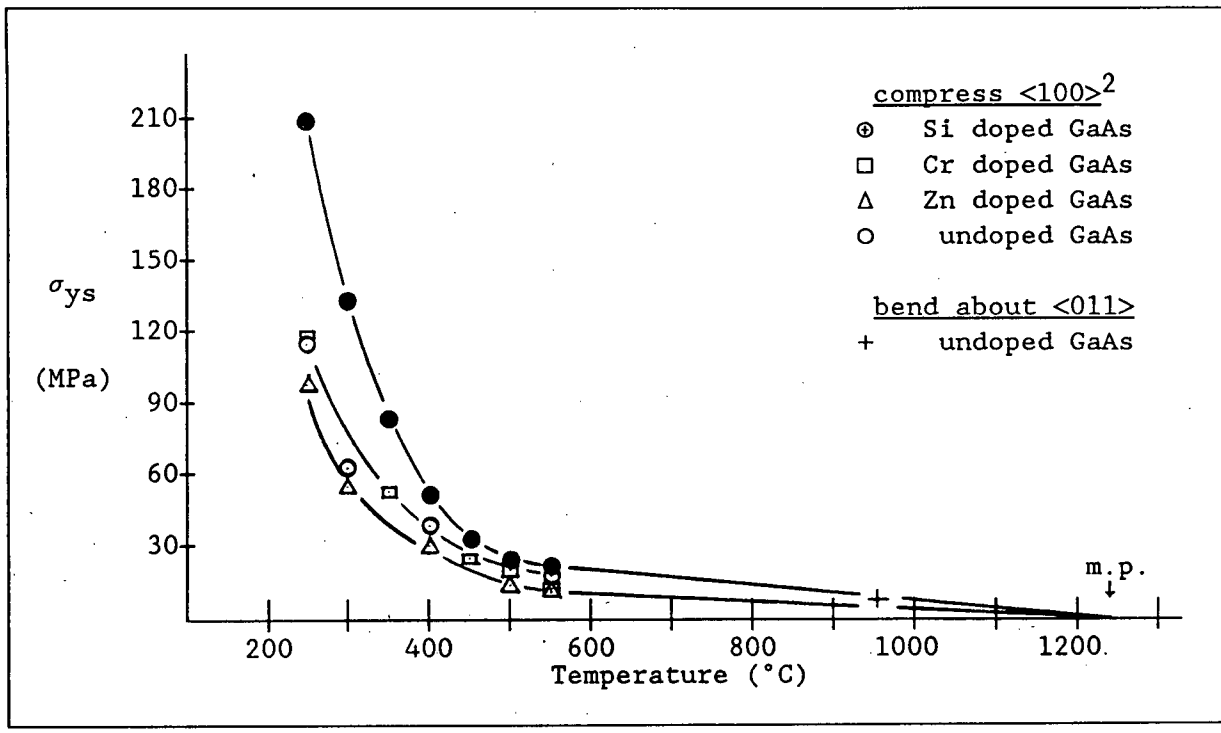

FIGURE 65. Yield stress versus temperature for doped/undoped GaAs tested in compression along <100> axis[2] and in bending about <011> axis.

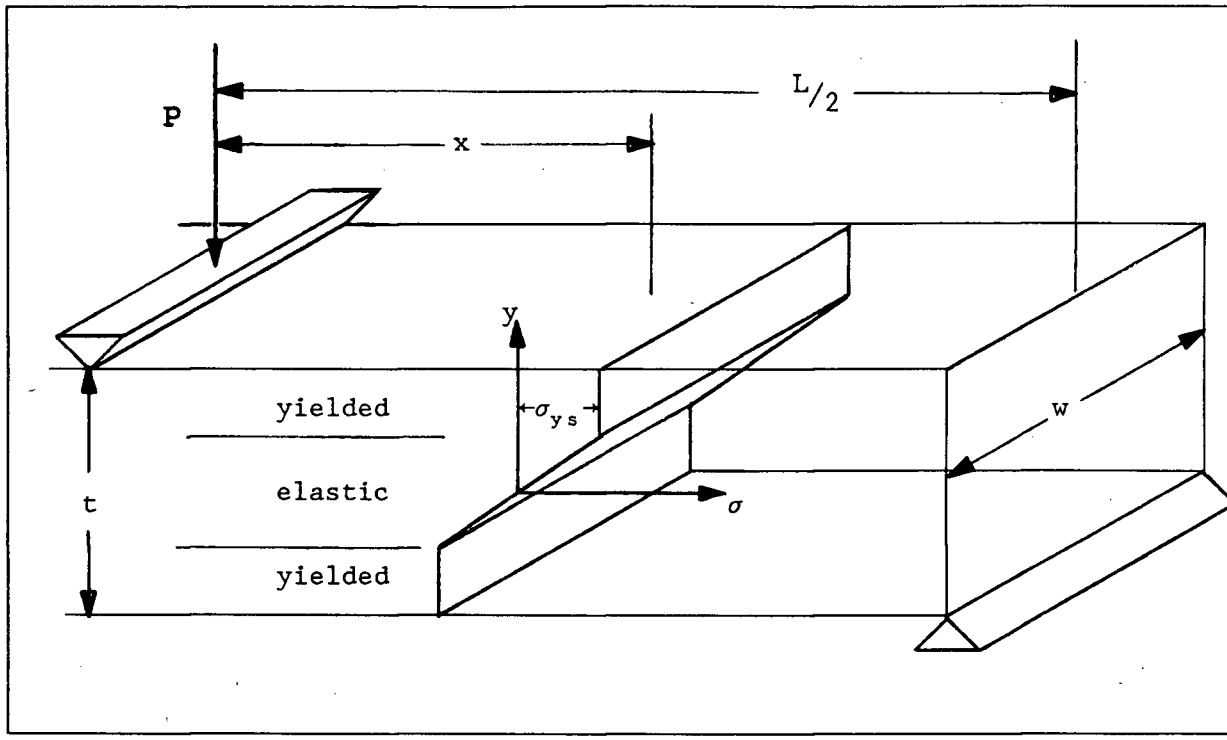

FIGURE 66. Construction showing stress distribution and yield depth (YD) in a 3-point bend specimen undergoing contained plastic yielding, a distance (x) from the centrally applied load (P).

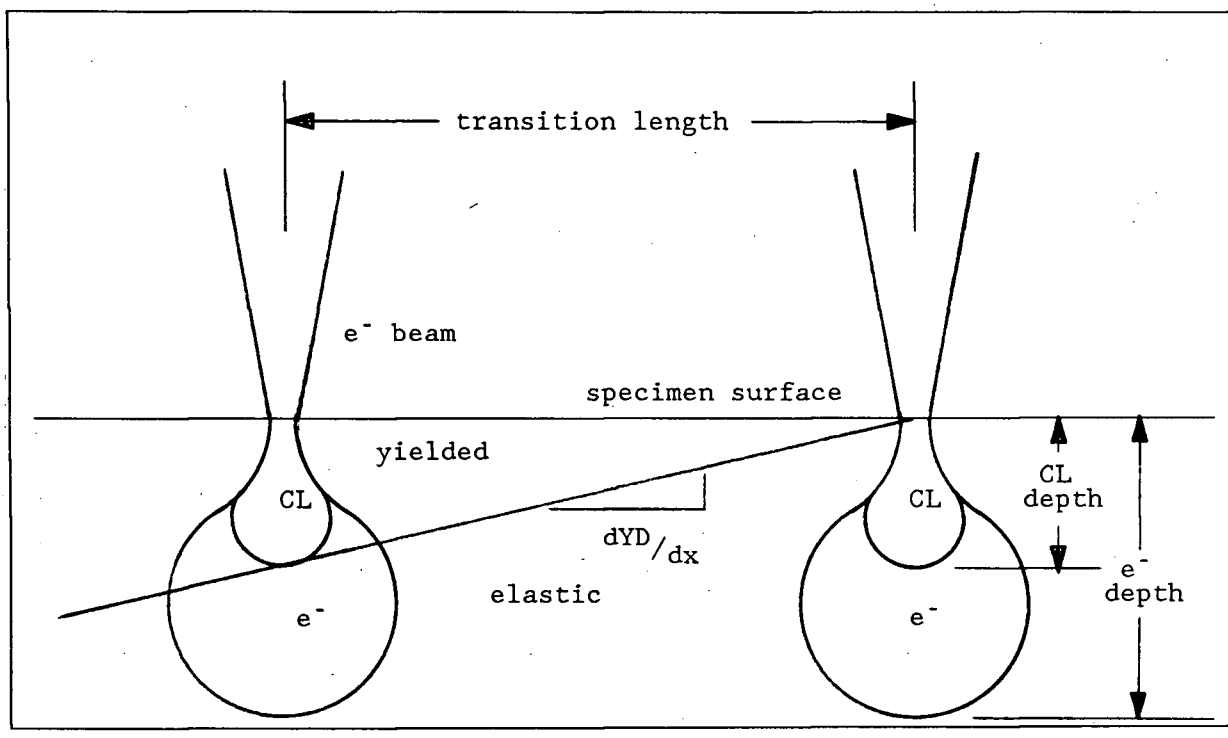

FIGURE 67. Schematic showing effective CL generation depth about the transition region in GaAs specimen S4.

List of References

1) D. Laister / G.M. Jenkins
"Deformation of a Single Crystal of GaAs"
Journal of Material Science
volume 8 number [9] pp1218-32 (1973)

2) V. Swaminathan / S.M. Copley
"Temperature and Orientation Dependence of Plastic Deformation in GaAs Single Crystals Doped With Si, Cr, or Zn"
Journal of the American Ceramic Society
volume 58 No. 11 - 12 pp482-485 (1975)

3) K. Maeda / M. Sato / A. Kubo / S. Takeuchi
"Quantitative Measurements of Recombination Enhanced Dislocation Glide in Gallium Arsenide"
Journal of Applied Physics
volume 54 number [1] pp161-168 (1983)

4) K. Maeda / S. Takeuchi
Japanese Journal of Applied Physics
volume 20 letter L165 (1981)

5) C. Kittel
"Introduction to Solid State Physics"
5th edition copyright 1976
John Wiley and Sons
p 530 (1976)

6) G.T. Brown / C.A. Warwick / I.M. Young / G.R. Booker
"An Examination of Dislocations in Si-doped LEC GaAs by Double Crystal X-ray Topography, SEM Cathodoluminescence and Chemical Etching"
International Physics Conference Series Number 67
Microscopy of Semiconducting Materials (1983)
The Institute of Physics pp371-377

7) T. Kamejima / F. Shimura / Y. Matsumoto /
H. Watanabe / J. Matsui
"Role of Dislocations in Semi-Insulation Mechanism in Undoped LEC GaAs Crystals"
Japanese Journal of Applied Physics
volume 21 number 11 pp L721-L723 (1982)

8) N.J. Shah / H.Ahmed / L.A. Freeman / D.J. Smith
"Electron microscopy of Se-implanted and electron-beam annealed GaAs"
International Physics Conference Series Number 67
Microscopy of Semiconducting Materials (1983)
The Institute of Physics pp125-130

M.A. Shadid / S. Moffatt / N.J. Barrett / B.J. Sealy
"Investigation of ion-implanted GaAs following electron-beam annealing"
Institute of Physics Conference Series Number 67
Microscopy of Semiconducting Materials 1983
The Institute of Physics pp131-136

10) C.A. Warwick / S.S. Gill / P.J. Wright / A.G.Cullis
"Spatial variation of dopant concentration in $^{29}Si^{+}$ implanted Czochralski and metal-organic vapour phase epitaxial GaAs"
Institute of Physics Conference Series Number 76
Microscopy of Semiconducting Materials 1985
The Institute of Physics pp365-372

11) D.B. Holt / S. Datta
"The Cathodoluminescent Mode as an Analytical Technique: Its Development and Prospects"
Scanning Electron Microscopy 1980
volume 1 pp259-278 (1980)

12) S.M. Davidson
"Semiconductor material assessment by scanning electron microscopy"
Journal of Microscopy
volume 110 part 3 August 1977 pp177-204 (1977)

13) E. Popov
"Introduction to Mechanics of Solids"
Copyright 1968
(Prentice-Hall Inc. Englewood Cliffs, New Jersey)
sections 6.8, 11.13, 12.8

14) D. Broek
"Elementary Engineering Fracture Mechanics"
Third Edition
Copyright 1983 Martinus Nijhoff Publishers, The Hague
pp 101-102

15) S.M. Davidson / C.A. Dimitriadis
"Advances in the electrical assessment of semiconductors using the scanning electron microscope"
Journal of Microscopy
volume 118 part 3 March 1980 pp275-290 (1980)